Bull Volcanol (1990) 52:426–444

Bulletin of
Volcanology

Evolution of the Quaternary melilite-nephelinite Herchenberg volcano (East Eifel)

Ulrich Bednarz and Hans-Ulrich Schmincke

GEOMAR, Wischhofstrasse 1-3, D-2300 Kiel 14, Federal Republic of Germany

Received December 1, 1989/Accepted April 17, 1990

Abstract. The Quaternary Herchenberg composite tephra cone (East Eifel, FR Germany) with an original bulk volume of $1.17 \cdot 10^7$ m^3 (DRE of $8.2 \cdot 10^6$ m^3) and dimensions of ca. 900·600·90 m (length·width·height) erupted in three main stages: (a) Initial eruptions along a NW-trending, 500-m-long fissure were dominantly Vulcanian in the northwest and Strombolian in the southeast. Removal of the unstable, underlying 20-m-thick Tertiary clays resulted in major collapse and repeated lateral caving of the crater. The northwestern Lower Cone 1 (LC1) was constructed by alternating Vulcanian and Strombolian eruptions. (b) Cone-building, mainly Strombolian eruptions resulted in two major scoria cones beginning initially in the northwest (Cone 1) and terminating in the southeast (Cones 2 and 3) following a period of simultaneous activity of cones 1 and 2. Lapilli deposits are subdivided by thin phreatomagmatic marker beds rich in Tertiary clays in the early stages and Devonian clasts in the later stages. Three dikes intruded radially into the flanks of cone 1. (c) The eruption and deposition of fine-grained uppermost layers (phreatomagmatic tuffs, accretionary lapilli, and Strombolian fallout lapilli) presumably from the northwestern center (cone 1) terminated the activity of Herchenberg volcano. The Herchenberg volcano is distinguished from most Strombolian scoria cones in the Eifel by (1) small volume of agglutinates in central craters, (2) scarcity of scoria bomb breccias, (3) well-bedded tephra deposits even in the proximal facies, (4) moderate fragmentation of tephra (small proportions of both ash and coarse lapilli/bomb-size fraction), (5) abundance of dense ellipsoidal juvenile lapilli, and (6) characteristic depositional cycles in the early eruptive stages beginning with laterally emplaced, fine-grained, xenolith-rich tephra and ending with fallout scoria lapilli. Herchenberg tephra is distinguished from maar deposits by (1) paucity of xenoliths, (2) higher depositional temperatures, (3) coarser grain size and thicker bedding, (4) absence of glassy quenched clasts except in the initial stages and late phreatomagmatic marker beds, and (5) predominance of Strombolian, cone-building activity. The characteristics of Herchenberg deposits are interpreted as due to a high proportion of magmatic volatiles (dominantly CO_2) relative to low-viscosity magma during most of the eruptive activity.

Introduction

In many fields of monogenetic basaltic volcanoes, eruptive mechanisms range from dominantly magmatic (Strombolian/Hawaiian scoria cones plus lava flows) to dominantly phreatomagmatic (Vulcanian) maars and tuff rings as inferred principally from the nature of the deposits and edifices. Mafic volcanoes of the Quaternary East Eifel volcanic field (EEVF) show all gradations between these two end members (Schmincke 1977a, b): (a) maars and tuff rings formed entirely by Vulcanian activity (e.g., Lummerfeld Maar); (b) scoria (agglutinate) cones entirely of Strombolian/Hawaiian origin (e.g., Ettringer Bellerberg, Tönchesberg), and (c) those in which phreatomagmatic (Vulcanian) and Strombolian/Hawaiian styles alternate such as at Rothenberg volcano (Schmincke 1977a, b, 1990; Houghton and Schmincke 1986, 1989). Herchenberg volcano consisting almost entirely of lapilli deposits allows us to evaluate another factor: the characteristics of deposits from eruptions of low-viscosity/high-volatile mafic magma.

Herchenberg volcano, situated about 5 km north of the Laacher See at the northern rim of the late Quaternary East Eifel volcanic field (EEVF, Figs. 1, 2), is largely composed of hauyne-bearing melilite-nephelinitic tephra. In the EEVF, some 100 volcanic centers have erupted in several major phases, which can be distinguished compositionally and spatially (e.g., Schmincke 1977b, 1991; Duda and Schmincke 1978). An older suite (> 400 000 years B.P.) of leucitites, melilite-nephelinites, and evolved rocks is concentrated in the western area of the EEVF (Rieden-Kempenich area). The younger subfield of the EEVF is dominated by scoria

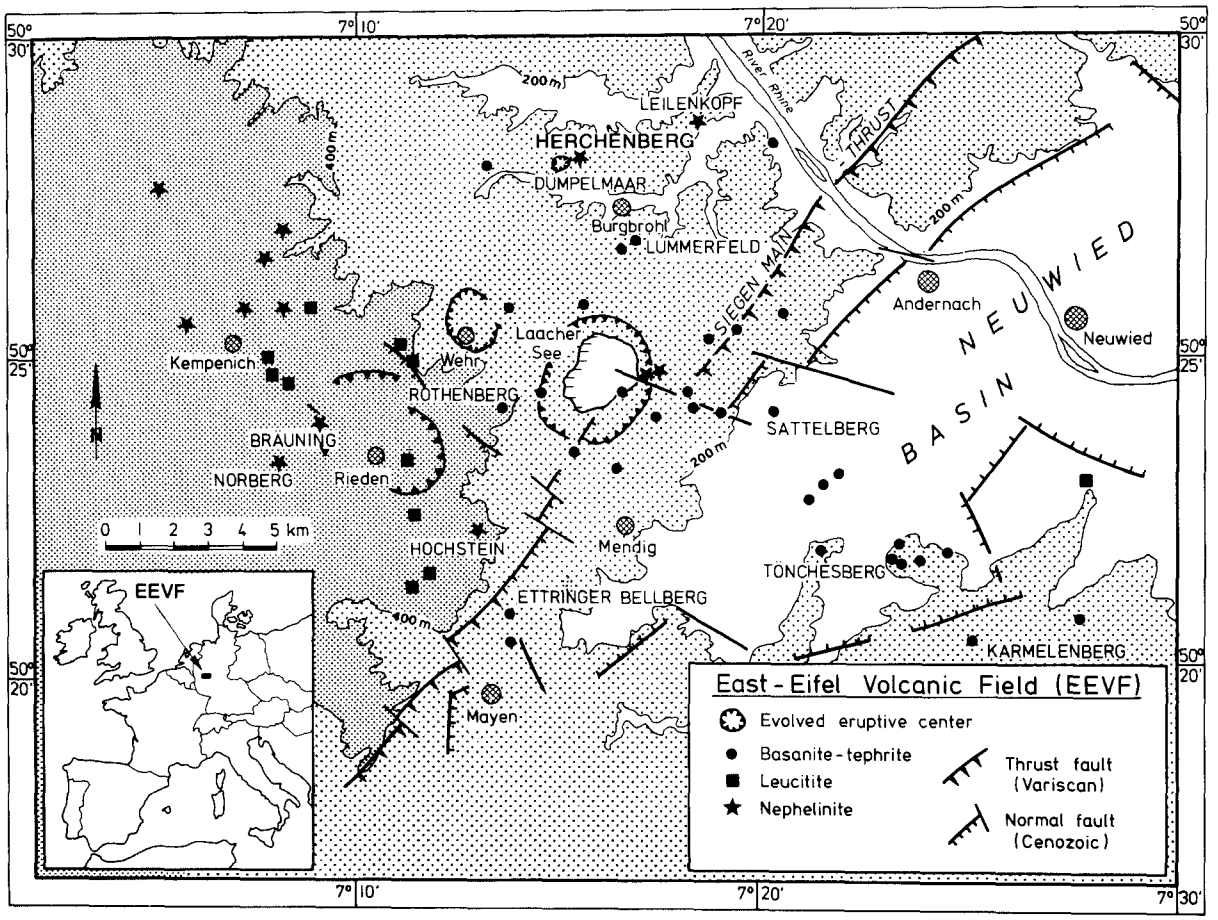

Fig. 1. Location map of the East Eifel volcanic field (*EEVF*) showing mafic volcanoes evolved eruptive centers and volcanic complexes

cones of basanitic to tephritic composition. The volcanic activity in the EEVF culminated in the eruption of ca. 5 km^3 DRE of Laacher See pumice about 11 000 years B.P. (e.g., Bogaard and Schmincke 1985).

Most previous work at Herchenberg volcano was concerned with tephrochronological aspects and is reviewed by Bednarz (1982). Here we will discuss the evolution of the volcanic complex. The origin of peculiar, ellipsoidal, dense lapilli is discussed elsewhere (Bednarz and Schmincke, in prep). Mineralogy, petrology, and magma properties are treated in Bednarz and Schmincke (in prep). Recent $^{40}Ar/^{39}Ar$ laser dating of Herchenberg phlogopites (Bogaard, unpublished data) indicates an eruptive age of approximately 480 000 years B.P.

The basement beneath Herchenberg volcano is made up of Lower Devonian (Siegenian) sandstones and slates with a total thickness of about 4 km (Meyer and Stets 1975); fold axes trend ENE-WSW. The weathered Devonian rocks are overlain in the Herchenberg area by about 20 m of Tertiary clays and sands topped by >2 m of Pliocene gravels ("Kieseloolitherrasse"), which form an important regional marker bed (Ahrens 1929; Fig. 3). Ahrens (1930) postulated a small local Quaternary tectonic collapse basin with up to 50 m subsidence around Herchenberg based on the low elevation of these gravel beds (ca. 220–235 m asl) compared with their regional elevation of approximately 270 m asl. Quaternary deposits around Herchenberg comprise loess, soils, and several tephra layers derived from other volcanic centers of the EEVF. Clastic dikes, dominantly phonolites, originated at the Dümpelmaar center 0.5 km southwest of Herchenberg (Bednarz and Schmincke, in prep) at 116 000 ± 16 000 years B.P. (Bogaard et al. 1987). Phonolitic Dümpelmaar tephra (DMT) overlies the Herchenberg scoria cone with a maximum thickness of approximately 6 m.

Petrology and geochemistry

Herchenberg lavas are phyric to glomerophyric, hauyne-bearing melilite nephelinites with 10–14 vol% clinopyroxene, 1–3 vol% olivine, 1–2 vol% hauyne, 1–4 vol% titanomagnetite, and <1 vol% phlogopite pheno- and microphenocrysts. Clinopyroxene, nepheline, melilite, and Fe-Ti oxides are the dominant groundmass phases. Accessory phases are microphenocrysts of carbonate and chrome spinel. Carbonate globules (ocelli) with maximum diameters around 0.2 mm occur mainly in the vitric groundmass of early lapilli. Patchy cemen-

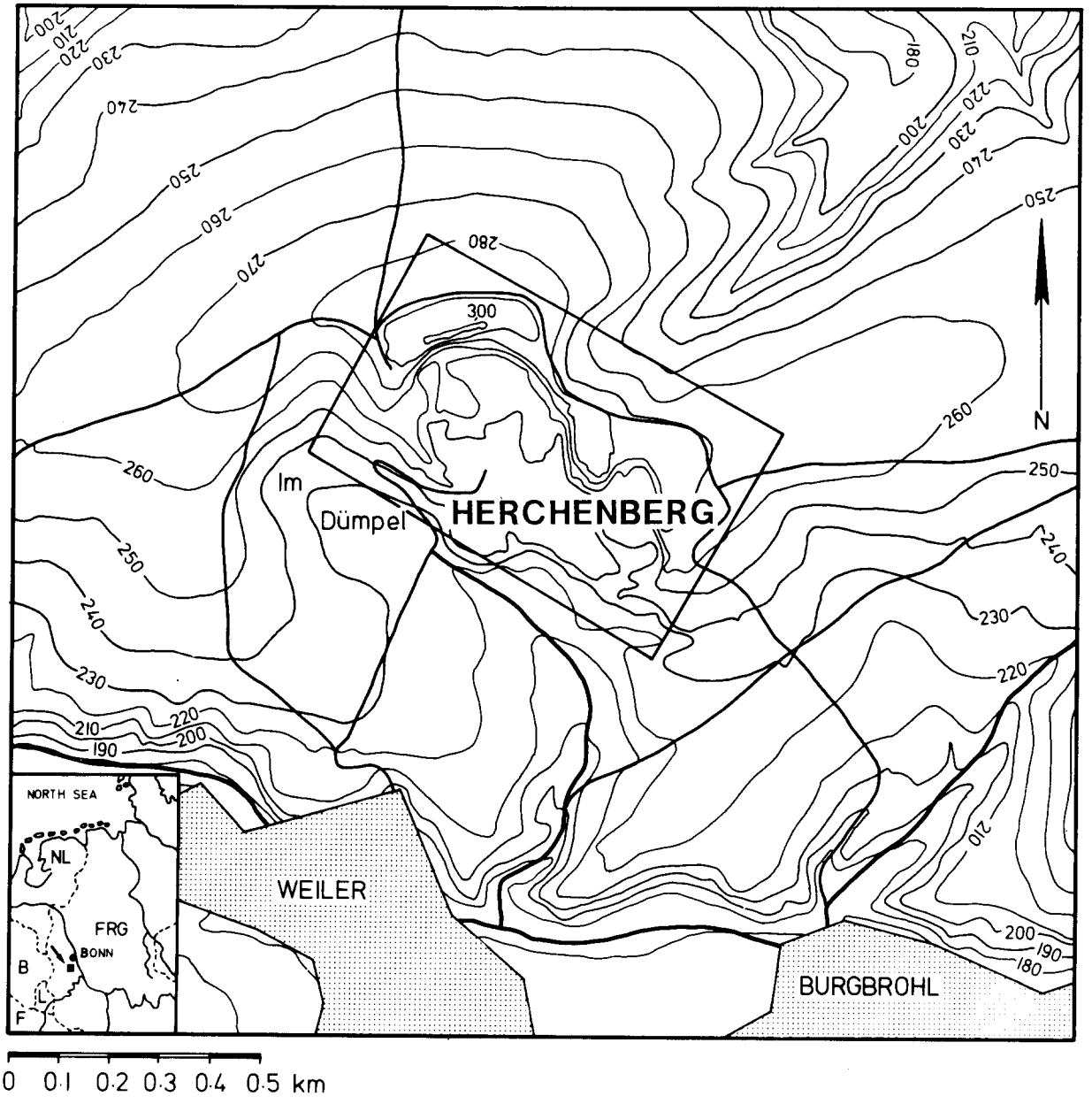

Fig. 2. Topographic map of the Herchenberg area. Frame indicates the position of the structural map of Fig. 4

tation by brownish sparry carbonate occurs locally in early lapilli layers. Phenocryst modes did not vary systematically during the evolution of Herchenberg volcano.

The chemical composition and chemcial variations of Herchenberg are distinctly different from the well-constrained chemical trends of the E-Eifel basanite-tephrite-phonolite series, which are related largely to fractional crystallization in intermediate- to high-level crustal magma chambers (Duda and Schmincke 1978; Schmincke 1982; Wörner and Schmincke 1984; Viereck 1984). The peculiar chemical trends observed in Herchenberg lavas may be largely explained by separation and fractionation of an immiscible carbonatite magma rich in Na_2CO_3, K_2CO_3, and $SrCO_3$ (Bednarz and Schmincke, in prep).

Structure of the volcano

The main quarry extends as much as 80 m deep into Herchenberg volvano (Figs. 2, 4) with exposed walls over >3 km long, thus permitting a detailed study of the stratigraphy of the deposits and structure of the volcanic edifice.

Eruptive centers were located using morphology, periclinal strike, crater wall unconformities, degree of welding, dikes, and systematic changes in grain size and thickness of marker beds.

Stratigraphy

Six main stratigraphic units are distinguished (Fig. 3): 1) initial deposits (massive phreatomagmatic and Strombolian facies);

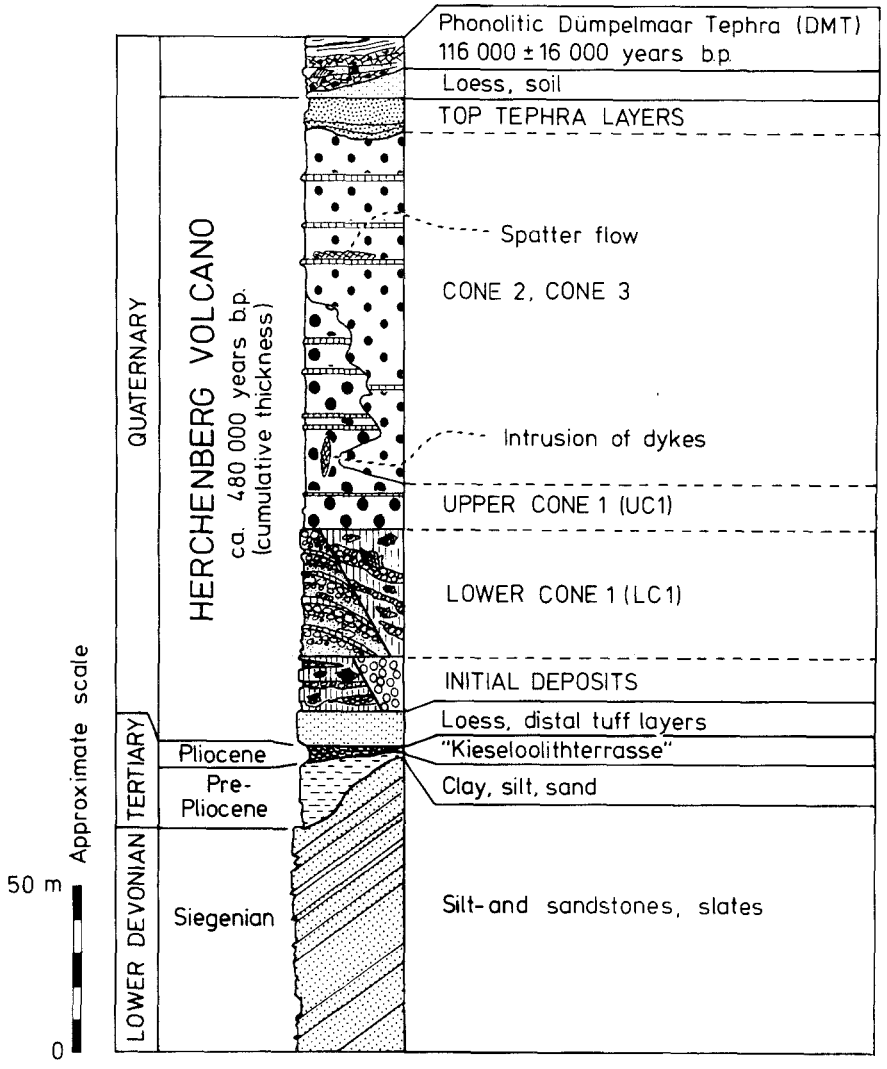

Fig. 3. Schematic columnar section of the stratigraphic succession at Herchenberg volcano (Tertiary after Ahrens 1929). $^{40}Ar/^{39}Ar$ single-crystal laser dates of Herchenberg and Dümpelmaar eruptions after Bogaard (unpublished) and Bogaard et al. (1987)

2) lower cone 1 (LC1), initial deposits (rhythmically bedded rim facies and more massive "channel" facies);
3) upper cone 1 (UC1), Strombolian and mixed Strombolian/phreatomagmatic facies;
4) cone 2 (C2), Strombolian facies punctuated by phreatomagmatic pulses;
5) cone 3 (C3), Strombolian, mostly welded facies inside the crater of cone 2 with minor nonwelded crater wall facies;
6) late top tephra layers covering the entire edifice.

The dikes most likely intruded the flanks of cone 1 during early stages of the construction of cone 2. Lava flows were not produced by Herchenberg volcano except for a 10-m-long spatter flow forming a small rampart during construction of cone 2 (Fig. 5).

The eruptive sequence

Initial deposits

The lowest exposed deposits of Herchenberg volcano in the south, southeast, and west dip 20°–45° toward the central crater forming an overall bowl-shaped structure. We interpret these volcano remnants as segments of the initial eruptive phases of Herchenberg volcano which were rotated toward the volcanic center due to major crater collapse during the early eruptive stages of Herchenberg volcano.

The initial tephra deposits comprise (I) a massive Vulcanian tuff-breccia facies in the south and west and (II) a Strombolian lapilli fallout facies in the south and southeast. Though poorly exposed, they are distinguished because:
(a) The deposits of the first well-exposed eruptive phase (lower cone 1; see below) postdate collapse and tilting of blocks into the crater area. The products of an earlier eruptive phase are mainly downfaulted below the present level of exposure.
(b) Strombolian fallout lapilli, which are also exposed in the southernmost part of the outcrops, are interpreted to be older than lower cone 1 as they
- are unlike any other deposit of Herchenberg volcano and
- have been strongly affected by volcano-tectonic events, most likely the early collapse of the crater area.

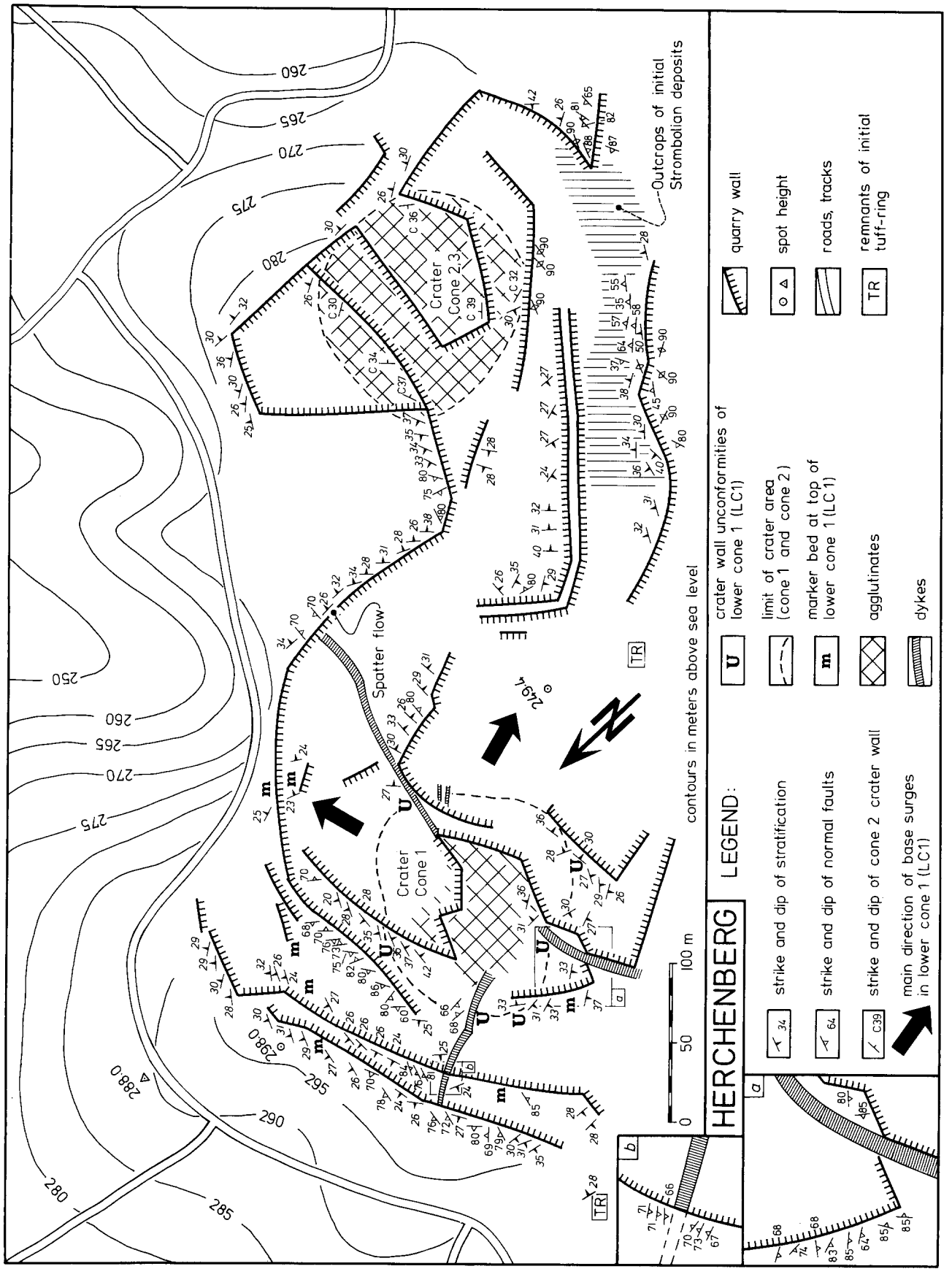

Fig. 4. Structural map of the Herchenberg quarry. Location shown in Fig. 2

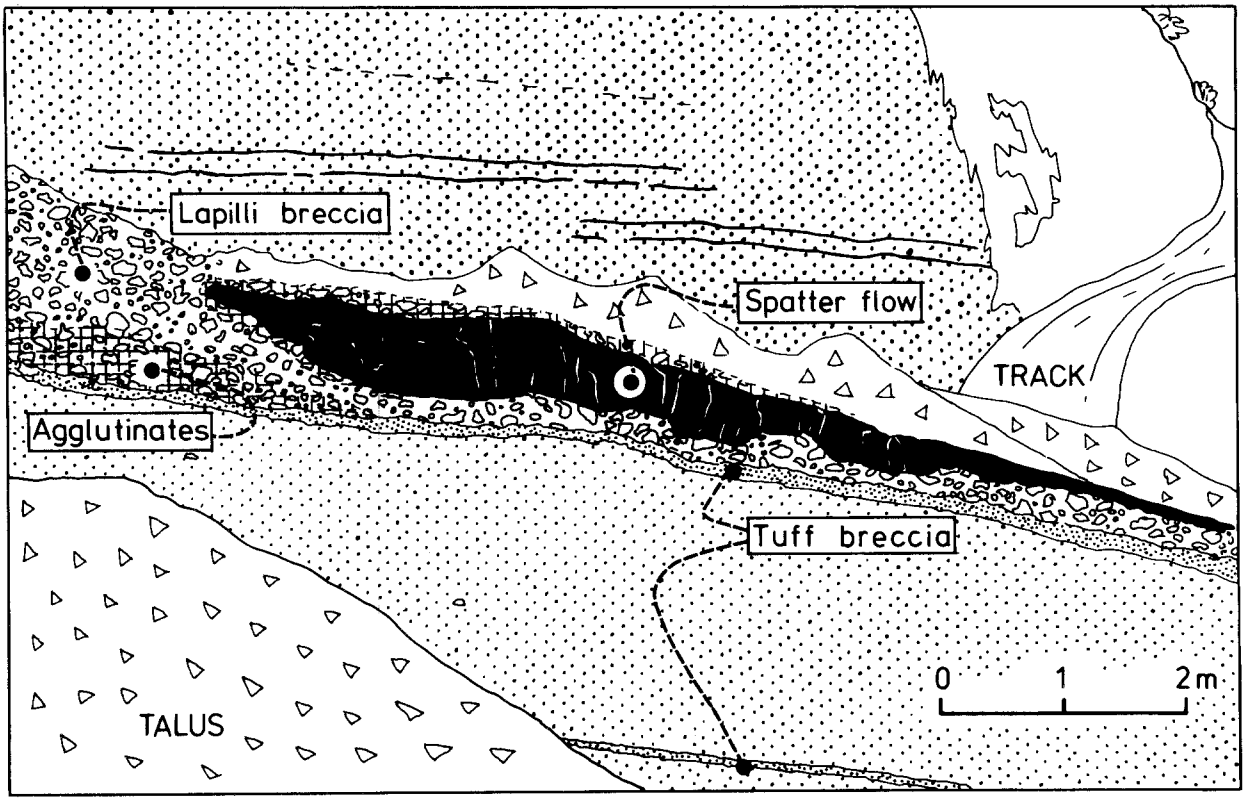

Fig. 5. Field sketch (looking east) of small spatter flow draining down the flank of cone 1 (into right background) in response to high local tephra accumulation rates during eruptions from cone 2 (see also Fig. 4)

These deposits are also older than the early phase of cone 2 deduced from direct depositional relationships. As cone 2 is partly contemporaneous with upper cone 1, it can further be definitely ruled out that these Strombolian deposits represent lower cone 1, which is characterized by abundant Vulcanian deposits; they must thus be older than lower cone 1.

1 Massive facies

The massive facies (minimum thickness of ca. 10 m), poorly exposed in the western and southern ends of the quarry (TR in Fig. 4), is made up of moderately bedded and poorly sorted Vulcanian tuffs, which contain >80% of xenoliths, chiefly near-surface Tertiary gravels, clays, silts, and sands. Quaternary loess and pumice clasts from the underlying distal Rieden tephra, Devonian slate and sandstone xenoliths are rare. Xenoliths range from <2 μm to blocks >0.5 m in diameter. Juvenile clasts are lapilli size with abundant fresh siderome-lane and may be enriched in thin lensoid layers.

2 Strombolian fallout facies

Strombolian fallout deposits of the Initial phases occurring in the south and southeast of the quarry are at least 15 m thick and composed of well-sorted, highly vesicular lapilli. Individual beds are as thick as 5 to 6 m and very homogeneous; single, inversely graded layers are about 20–50 cm thick. Average grain sizes range from 1–2 mm at the base to 0.5–1 cm at the top. Initial Strombolian fallout deposits are nearly xenolith-free. Some of the strongly thermally modified ("inflated") crustal xenoliths up to about 10 cm in diameter are well rounded. Phlogopite crystals are mostly thickened and distorted by extreme carbonatization. While intergrowths of carbonate and phlogopite occur throughout the Herchenberg scoria, they are rare in the younger eruptive products and are nowhere as intense as in the initial Strombolian deposit.

The contact between the basal Tertiary silty sands and clays and the initial pyroclastic deposits is exposed at the southwestern base of the volcano (Fig. 3): (I) a volcano-tectonic contact dipping 80° to the northwest, and (II) an almost concordant contact, dipping 45° to the northeast. Tectonic contacts include those between tephra/tephra, Tertiary sediments/tephra, and Quaternary sediments/tephra. The maximum angles of dip of tephra layers are up to 50°, much too steep for primary deposits. These abundant faults are interpreted to have resulted from collapse of the marginal crater area in the unstable Tertiary basement during the initial eruptive stage.

Lower cone 1 (CL1)

An area with nearly closed periclinal strike of tephra layers (cone 1) occurs in the northwest (Fig. 3). The crater wall, unusual among Eifel cones, is essentially

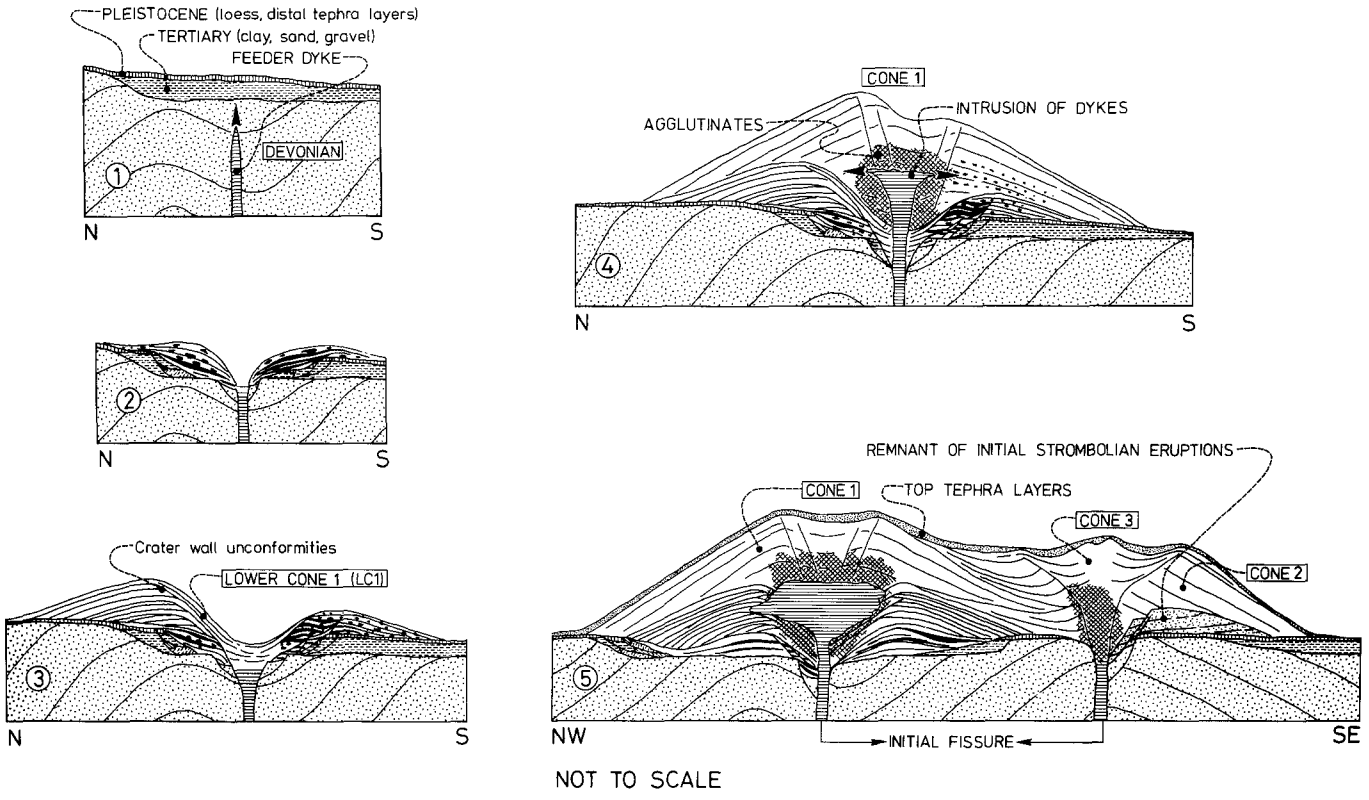

Fig. 6. Cross sections showing 5 evolutionary stages of Herchenberg volcano. Stages 1–4 show NS cross sections through cone 1. Stage 5 shows a cross section along the inferred initial eruptive fissure trending northwest-southeast. **1,** Pre-eruption rise of magma through a fissure in Devonian basement capped by up to 20 m of Tertiary clays. Quaternary layers comprise loess, soil, and distal tephra probably derived from the Rieden complex (Fig. 1). **2,** Initial, dominantly phreatomagmatic eruptions in the northwestern part are characterized by low eruption clouds and ejection of xenolith blocks on low-angle ballistic trajectories. Tertiary clay is excavated and repeatedly faulted at the vent flanks. **3,** Lower cone 1 (LC1) is characterized by a rhythmic depositional cycle with Strombolian deposits dominating in the north and phreatomagmatic deposits containing large blocks of Tertiary clay dominating in the northeast and south. **4,** Formation of upper cone 1 (UC1) is dominated by Strombolian eruptions and is partly contemporaneous with the erection of cone 2 (stage 5). During this period three major dikes intruded the flanks of cone 1. **5,** The northwest-southeast cross section shows interlayering of cone 1 and cone 2 deposits. Within the crater area of cone 2 (enlarged by collapse?) the small cone 3 formed whose deposits do not reach far over the flanks of cone 2. Late tephra, probably originating from cone 1, covers the entire Herchenberg volcano edifice

constructional with repetitive minor unconformities. Layers dipping into the crater overlie older outward-dipping layers that compose the outer wall but may extend some way into the crater (Figs. 3, 6). Average dip into the crater is 24°, while the dip of the outer flanks of cones 1–3 averages around 35°.

In the lower part of cone 1, distinct radial, vertical, and in part lateral facies changes occur.

Northwestern sector (ca. 250°–40°)

The maximum height of LC1 in this sector is 40 to 50 m at the crater rim. Tephra is made up largely of well-bedded lapilli, forming graded beds comprising two different end-member bed types best developed on the outer slopes (Figs. 7, 8):

(a) Very thinly to thinly (1–10 cm) bedded, fine-grained, yellowish to reddish layers contain about 30 wt% xenoliths of mostly Tertiary sediments and form the sharp base of a bed. Along the crest of the crater wall, these layers generally rest unconformably on the eroded sur-

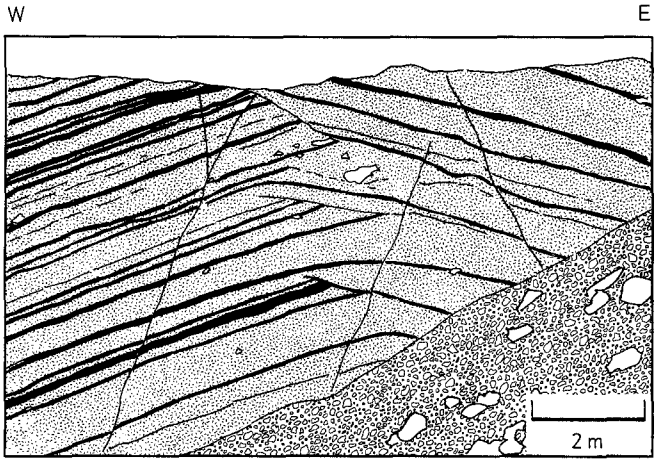

Fig. 7. Field sketch of a radial cross section through the crater wall in the northwest sector of lower cone 1 (LC1) showing crater wall unconformities. *Left:* outer flank of the cone; *right:* eruptive center of cone 1. Dark shading: thinly bedded tuff layers of bed type a forming the base of each depositional cycle and resting unconformably on the eroded surface of the underlying bed. Light-gray shading: thinly to moderately bedded green to black, mostly inversely graded lapilli layers of bed type b

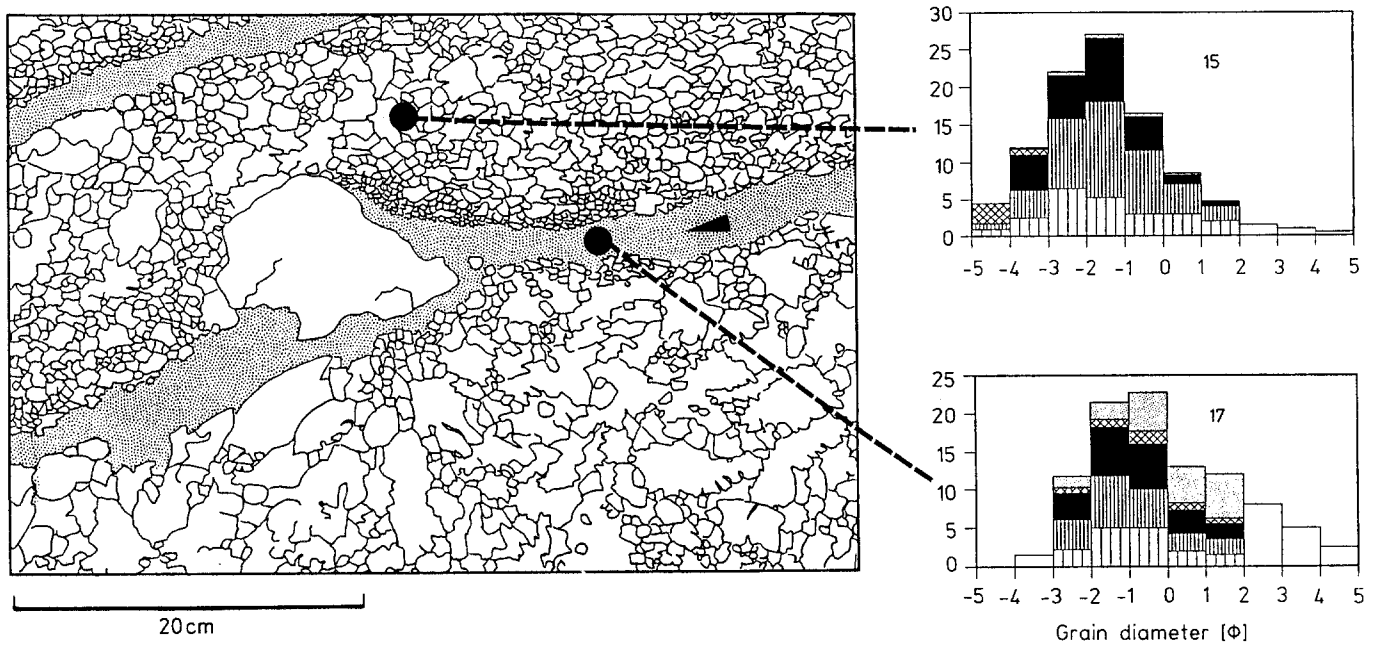

Fig. 8. Detailed sketch of bed types in the northwestern sector on the outer flanks of lower cone 1 (LC1) close to the crater wall (Fig. 7). Gray shading: thin reddish tuff layers (type a). Accretion against small bomb indicates transport in highly dispersed base surges to the left (*arrow*). Lapilli layers are inversely graded in clast size and normally graded in clast density, indicative of the development of a Strombolian eruption after each phreatomagmatic pulse. Histograms show grain size distribution and representative composition of bed types (a; sample 17) and (b; sample 15). For legend see Fig. 9

face of the underlying bed. Accretion against obstacles as well as bomb sags indicate a high water content of the fine-grained tephra during deposition. Both features, however, are rare because of the generally small grain sizes (Md_Φ 1.3 Φ) in the lower part of cone 1. Only 16 wt% of the essential clasts are vesicular.

(b) Thinly to moderately bedded (<30 cm) green to black layers with slightly wavy bedding planes contain <5 wt% Tertiary and Devonian xenoliths. They are commonly reversely size graded combined with a normal density gradient of the clasts, i.e., particles of higher density tend to be concentrated in the lower parts of the beds. These features, however, are restricted to the outer slopes, starting approximately 15 m from the crater wall, while beds on the inner slopes are not graded. Thickness of beds is reduced by about 0.5 at the rim. Md_Φ is around -2.5 Φ with a sorting coefficient σ_Φ of about 1.6; vesicular clasts normally make up >20 wt%.

Northeastern sector (ca. 40°-100°)

About 60 m from the crater rim, this facies resembles the Vulcanian beds of the initial deposits with respect to its massiveness, small grain size, poor sorting, and abundance of xenoliths. Xenolithic blocks of Tertiary clay up to 0.8 m long are common, while Devonian xenoliths are smaller (max. diameter 0.3 m) and rare. Oxidation of abundant fine-grained Tertiary xenoliths gives the whole deposit a bright reddish to orange colour. Juvenile lapilli generally appear in discontinuous, undulating lenses indicating synsedimentary mobilization due to the high water content of the phreatomagmatic tephra. Thickness and relative proportion of massive red tuff layers increase gradually in this sector from north to east. The absolute and relative thickness of reddish, massive, tuff-breccia layers within the northeastern sector increases to the east.

The overall abundance of black Strombolian fallout lapilli beds increases only in the upper part of LC1. The deposits of LC1 end with a sequence of up to 2.50 m of black, Strombolian, xenolith-poor fallout beds which are directly followed by a 1-2-m thick marker bed ("m" in Fig. 4) rich in Tertiary xenoliths (up to 0.8 m long). The latter can be followed around the northwestern sector covering an angle of about 180°.

Lateral facies changes within the northeastern sector cannot be traced directly as the quarry does not provide radial walls. However, over a period of about 8 years quarry operation proceeded for about another 40 m further away from the crater rim. The maximum size of Tertiary clasts and the relative proportion of massive phreatomagmatic tuff/breccia beds decreased considerably compared to the more proximal exposures. The entire deposit shows more pronounced and "better-organized" bedding.

Southern sector (ca. 100°-250°)

The proximal facies in the southern sector of LC1 is poorly exposed on the quarry floor. The increase in abundance and size of Tertiary clasts indicates that the facies in the south is similar to that in the northeastern sector, i.e., more massive Vulcanian. Massive tuff-brec-

cia beds increase in thickness downslope (by about a factor of 2 over a distance of approximately 10 m).

At a former higher level of exposure, the reddish, massive tuff-breccias of the south sector were bounded sharply to the southwest by a major steeply dipping fault, striking around 130°, parallel to the inferred initial fissure.

The total height of the crater wall up to the top of LC1 is approximately 20–30 m lower than in the northwestern sector, which is probably partly due to a pre-existing slope dipping to the south. It is, however, suspected that prevailing southerly winds during the eruption resulted in deposition of dominantly Strombolian products in the north leading to higher near-crater deposition and accumulation rates and a higher crater wall.

The whole section of LC1 is estimated to be about 8 m thick approximately 200 m from the crater rim at the southern end of the quarry. The sequence is dominated by yellowish-brownish tuff breccias, while mostly xenolith-poor lapilli fallout layers with high contents of highly vesicular lapilli comprise about 40% of the total thickness.

Upper cone 1 (UC1)

The northern and southern portions of the upper part of cone 1 show distinct differences. The boundaries between the sectors are not exposed due to the extensive quarrying.

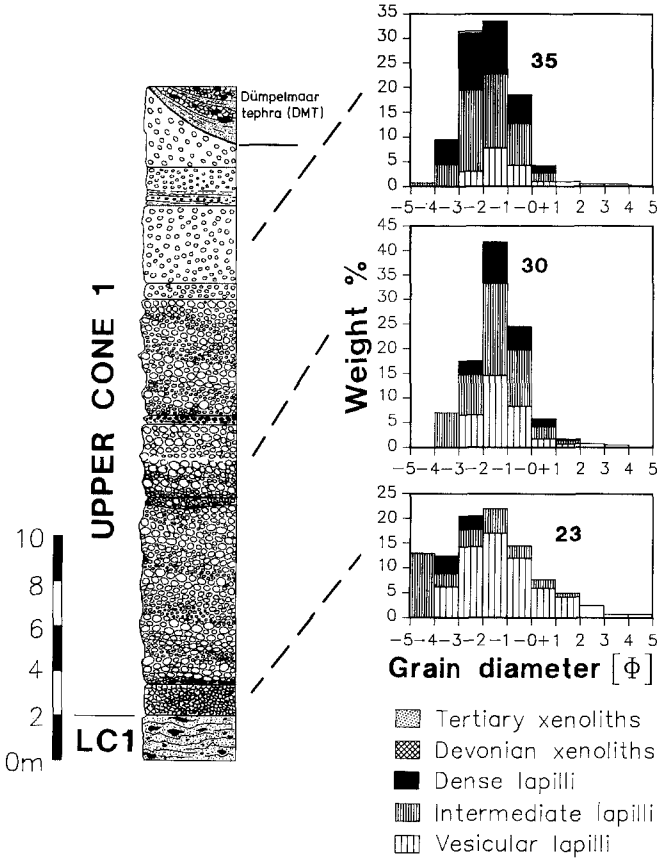

Fig. 9. Composite stratigraphic section of upper cone 1 in the northern sector 10–60 m from the crater wall. Histograms show grain size distribution and components of representative layers

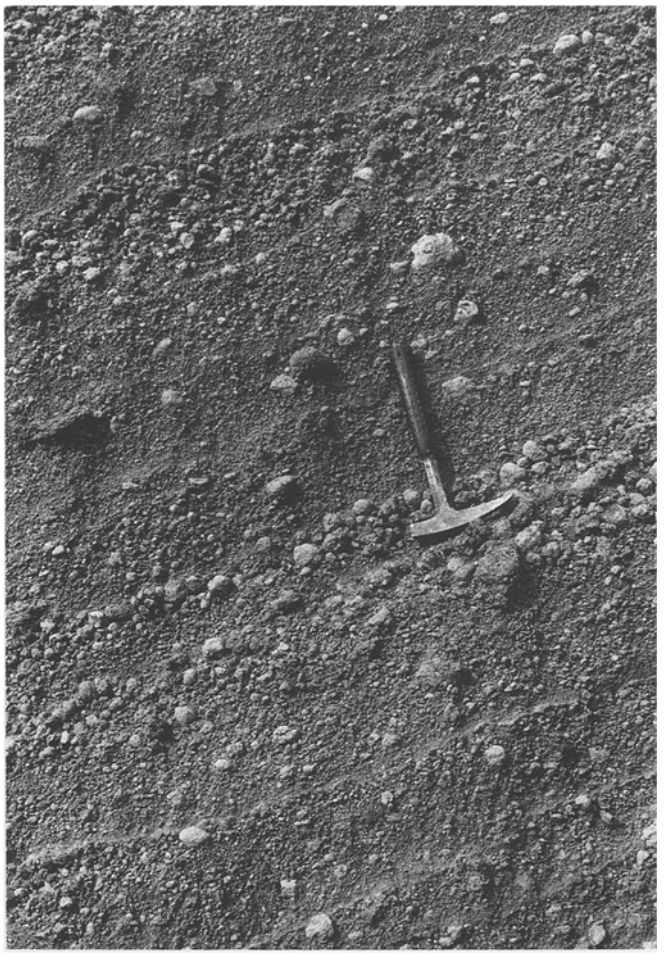

Fig. 10. Photograph of inversely graded lapilli layers in cone 2. Dense ellipsoidal lapilli are enriched in lensoid wedges indicating slumping and rolling of clasts on the outer flanks of the volcano. Hammer for scale

Northern sector

The upper part of cone 1 completely lacks the rhythmic depositional cycles in the northern sector (Fig. 9). It begins with a bed of scoriaceous lapilli, up to 1.5 m thick, containing about 75 wt% vesicular lapilli, and is intercalated with layers of lower cone 2 in the eastern and northeastern sector of cone 1, indicating a period of contemporaneous activity of both major Herchenberg eruptive centres.

The upper 30 m are mainly made up of medium to thickly (generally <1 m) bedded lapilli layers with <1 wt% xenoliths. The relative proportion of vesicular lapilli ranges 8–35 wt%. Common reversely graded bedding and strongly undulating bedding planes most likely resulted from repeated rolling and slumping of the dense scoria lapilli on the flanks of the volcano, which became unstable when increasing amounts of tephra was loaded on the upper slopes (cf. stage 4 of scoria cone model in McGetchin et al. 1974). This pro-

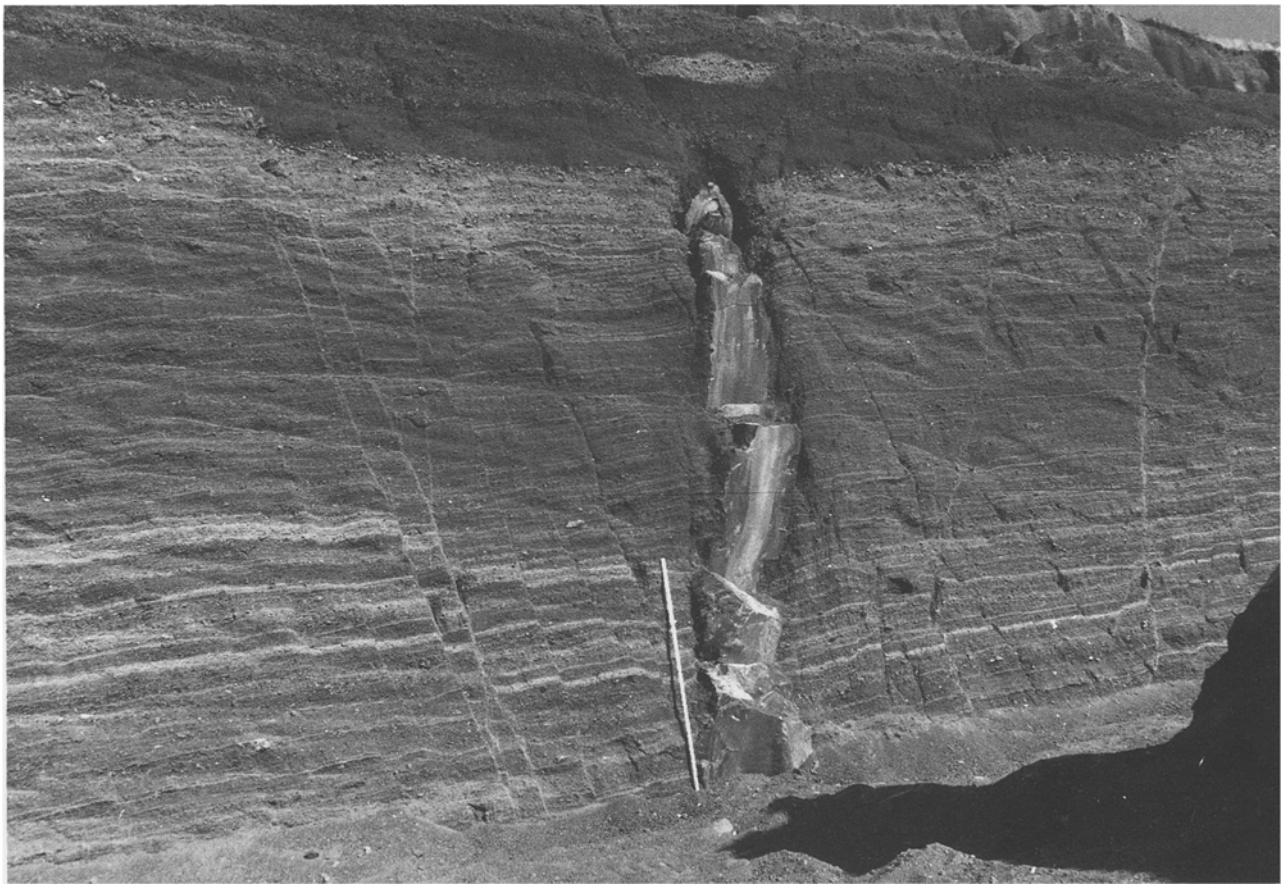

Fig. 11. Photograph of dike I, looking north toward the flanks of cone 1

cess was facilitated by the ellipsoidal shapes and smooth contours of up to 35 wt% of the pyroclasts, which are often found concentrated in wedge- and lensoid-shaped gullies (Fig. 10). Smaller particles may also fall through interparticle voids of larger ones and thus create the appearance of reverse graded bedding (Duffield et al. 1979). The effectiveness of the downslope rolling of particles is well illustrated in an exposure at the western margin of the quarry where the layers of cone 1 change the direction of dip and form a small trough while following the older morphology. Large lapilli and bombs with above-average diameters are restricted to the eastern, true cone slope while maximum clast sizes (up to 25 cm in diameter) are found within the narrow range of the morphological trough. On the opposite western E-dipping slope, maximum and average clast sizes decrease sharply.

Southern sector

Exposures in the southern sector of UC1 are limited. Distinct facies changes are, however, obvious. Beds are homogeneous and crudely bedded, while juvenile Strombolian clasts are smaller than in the northern sector. Reverse grading in some beds, 0.3–1 m thick, is not as distinct as in the northern sector. Slightly oxidized, reddish Tertiary clasts up to about 50 cm in diameter are abundant (5%–10%). Devonian xenoliths are rare and do not exceed about 5 cm in diameter. The whole deposit is reddish in color, probably due to small amounts of interspersed, fine-grained Tertiary xenoliths. Tertiary xenolith bombs are not dispersed throughout the deposits but in moderately distinct layers in which a particular particle size of xenoliths dominates (e.g., < 10 cm, ± 10 cm, 20–30 cm). Massive phreatomagmatic tuff layers as in LC1 do not occur.

Dikes

A system of three major radikal dikes intruded the flanks of cone 1, presumably during eruption of the upper part of cone 1 and early phases of cone 2. Dikes are vertical and exposed for a maximum length of about 150 m. They follow a gentle curvature resembling *en echelon* offsets resulting in slightly variable strikes: dike I, 138°–155°; dike II, 90°–98°, dike III, 60°–83°. Near-vent widths are up to about 5 m; the vertical height of exposure exceeds 10 m.

Evidence for partial magma drainback at least from dike I comes from a partially emptied dike tip and a zone, about 10 cm wide, close to the margin of the dike where elongate vesicles, which are otherwise oriented parallel to the dike margin, are sheared forming an angle of about 45° to the dike margin. Furthermore, the

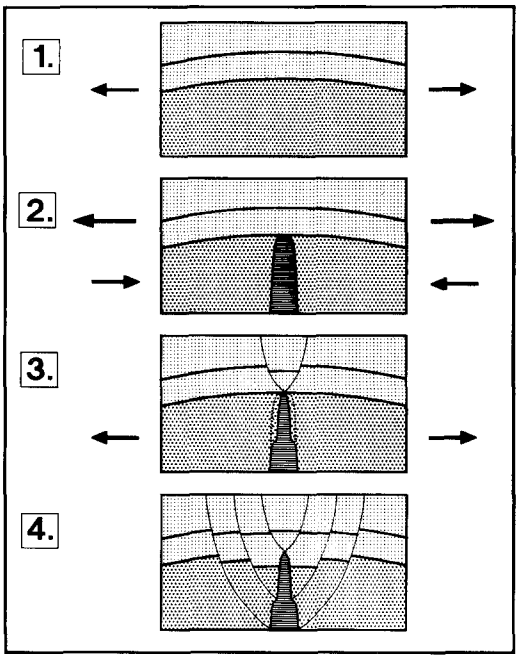

Fig. 12. Stages of intrusion of radial dike I into the flanks of lower cone 1 (LC1, dark shading) in four cross sections tangential to the cone structure. *Arrows* indicate orientation of stress field; length of arrows indicates relative size of the stresses. *1,* Pre-intrusion tensional stress field. *2,* Intrusion of dike results in a stronger tensional stress field over the tip of the dike and a relative compressional stress field at the side of the dike. *3,* This results in graben formation in the tip of the dike. *4,* Partial drainback of magma from the dike leads to graben formation on the flanks of the dike

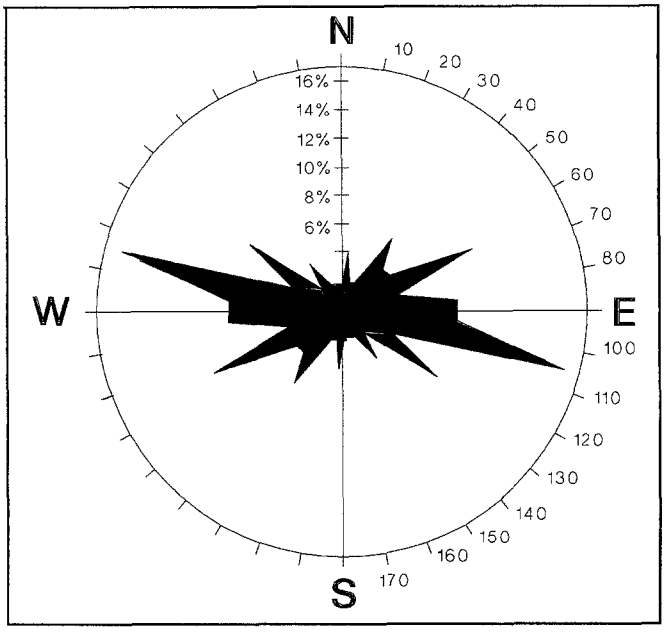

Fig. 13. Rose diagram showing relative frequency of strike of 82 small-scale normal faults in the Herchenberg cones and initial deposits

formation of a small (on the order of decameters), graben-like fault system about the dike (Figs. 11, 12; stage 4) may be explained by a volume/width decrease of the dike due to magma drainback.

Only dike I is partly oriented subparallel to the inferred initial fissure connecting cones 1 and 2 (135° ± 20°). We thus believe that these dikes do not represent feeders for the eruption of Herchenberg volcano, but intruded the flanks of the scoria cone more or less horizontally from the central crater area of cone 1. The tectonic stress field which dominates the orientation of the dikes is thought to be purely local resulting from the gravitational burden mainly of cone 1. The strike of 82 small-scale normal faults in the Herchenberg is roughly east-west (Fig. 13), subparallel to the directions of dikes II and III.

Cone 2 (C2) and cone 3 (C3)

The inner crater wall is well-exposed in the southeast. Layers of cone 3 are banked against the steeply dipping inner crater wall that most likely had formed by collapse. This type of crater unconformity separating an outer older wall from a younger inner filling is common in East Eifel scoria cones (Schmincke 1991).

Cone 2 and 3 deposits closely resemble the upper part of cone 1 and are made up mainly of reversely

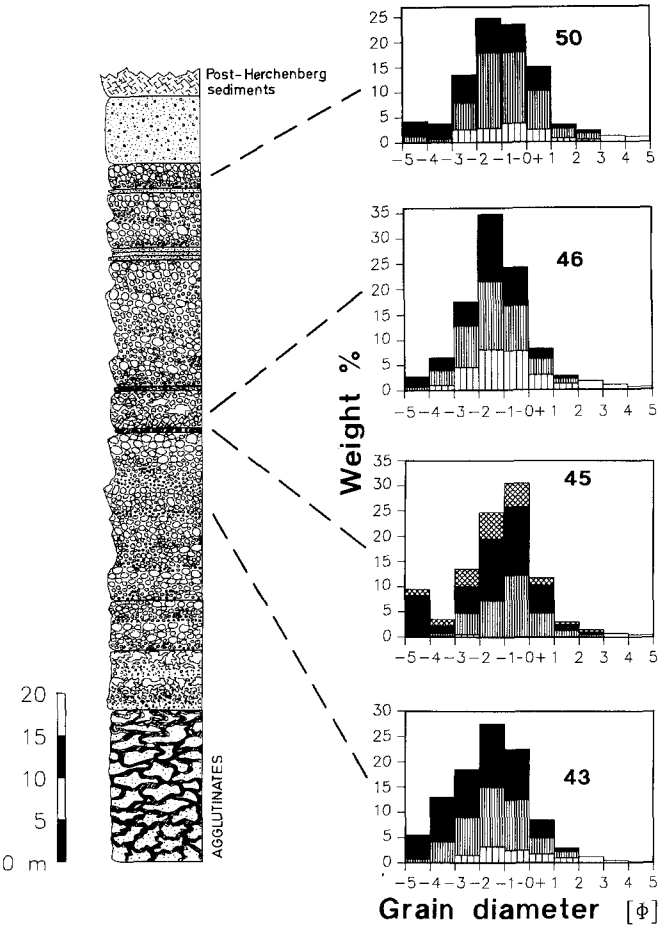

Fig. 14. Stratigraphic section of northern cone 20–50 m from the crater wall unconformity. Histograms show grain size distribution and components of representative layers. For legend see Fig. 9

graded, thinly to thickly bedded lapilli layers with slightly undulating bedding planes becoming increasingly discontinuous upsection. Vesicular lapilli make up only 1–27 wt% of these layers (Fig. 14); the lowest content was found in a marker bed of phreatomagmatic origin in cone 2 with approximately 20 wt% Devonian xenoliths, the highest in a directly overlying, homogeneous, non-stratified lapilli breccia with a maximum thickness of 15–20 m. In this layer, juvenile clasts are drastically larger than in the rest of cone 2. About 150 m northwest of the crater rim, a small rootless spatter lava flow is exposed close to its base (Figs. 4, 5), which is also characterized by large clasts. The lava flow is situated where cone 2 deposits overlie those of cone 1 and thus dip toward cone 2. The flow, which has a highly irregular base and a rather flat top, is about 10 m long and reaches its maximum thickness of about 1.5 m upslope thinning out quickly to the south (Fig. 5).

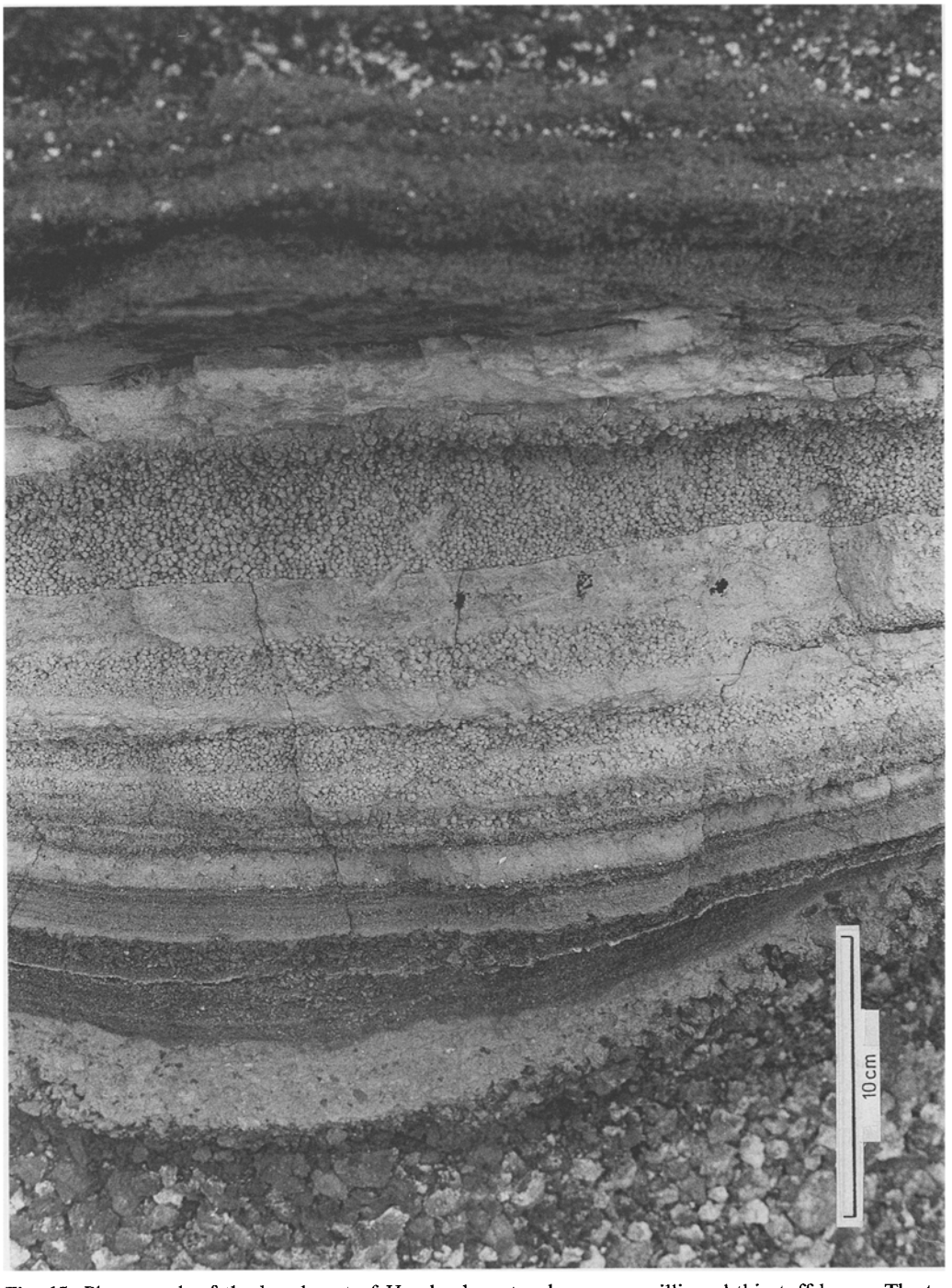

Fig. 15. Photograph of the basal part of Herchenberg top layers shows a sequence of thin, well-bedded layers of black, well-sorted, fine-grained lapilli, layers of well-sorted accretionary lapilli, and thin tuff layers. The top part of the outcrop is made up of black, well-sorted Strombolian fallout lapilli

We relate the formation of this flow to a short interval of lava fountaining with local accumulation rates high enough for intense welding and remobilization.

Overall xenolith contents in cones 2 and 3 are <1 wt%, despite a few 10–20-cm-thick tuff marker beds of phreatomagmatic origin in cone 2 where Devonian clasts may reach about 50 wt%. Ellipsoidal lapilli make up as much as 50 wt% of the distinct layers and are even more enriched in lensoid slump lobes (Fig. 10). Remarkably, reverse grading also developed in slightly welded pyroclastic breccias near the crater wall of cone 2. It thus seems unlikely that this phenomena is solely due to sorting processes during slumping, but must be produced by changes in eruptive dynamics.

Late tephra beds

Primary top layers comprise a sequence of up to 3 m thick, fine-grained lapilli, tuffs, accretionary and mantled lapilli which are well-bedded on a centimeter scale. Reworked sequences resulting from rain wash/erosion (cinder cone degradation) rapidly increase in thickness downslope to >10 m.

The base of the top layers fills a series of radial gullies 0.5–1 m wide and 20–50 cm deep. The lowermost tuff and lapilli layers are thick in the gullies indicating transport via mass flows. We do not completely rule out reworking for these lowermost layers, though this seems unlikely, as layers of extremely well sorted, delicate accretionary lapilli, which occur intercalated in these top layers, are definitely in situ (Fig. 15).

Accretionary lapilli range almost exclusively 1–5 mm, in size. Fine-grained tuff matrix is completely missing. Most accretionary lapilli consist of a relatively thick core made up of a vitric juvenile clast, an isolated phenocryst, or Devonian xenolith covered by a relatively thin mantle of fine-grained material mostly <200 µm. This type os small accretionary lapilli with relatively large cores typically make up to 85% of tephra layers (even in proximal facies), which were deposited from wet pyroclastic surges (base surges) according to Schumacher (1988) and Schumacher and Schmincke (1990).

Moderately welded spatter and dense agglutinates form the core areas of all three cones. In cone 1, agglutinates are restricted to the central inner crater area. In cone 2, slightly welded scoria layers extend some 10 m out of the crater, while much of the crater fill of cone 3 consists of agglutinates. The crater volume occupied by welded spatter in the Herchenberg (especially cone 1) is small compared to other E-Eifel tephra cones where intense welding may extend for more than 50 m outside the crater wall. This is taken as evidence for comparatively low emplacement temperatures of Herchenberg tephra even close to the inner crater.

Dimensions and volume

The dimensions of cones 1 and 2 were obtained by extrapolation of the most elevated pyroclastics with their proper did angle up to the assumed position of the crater wall (also obtained by extrapolation) and down to the elevation of the Pliocene alluvial terrace. The following dimensions were estimated:

Cone 1: basal width (W_{Co}), 500–600 m
height (H_{Co}), 80–90 m
H_{Co}/W_{Co}, 0.13–0.18
Cone 2: basal width (W_{Co}), 300–450 m
height (H_{Co}), 50–70 m
H_{Co}/W_{Co}, 0.14–0.22

The dimensions of cone 3 are relatively small as it is restricted by the space provided by the crater of cone 2 and probably did not rise significantly above the flanks of cone 2. In volume estimates, it is thus treated as the "core" of cone 2.

Wood (1980b) and Porter (1972) found critical values for the H_{Co}/W_{Co} ratio for young scoria cones of 0.15 and 0.179, respectively. Our estimates for Herchenberg volcano range within these values. Crater width (W_{Cr}) is obtained from Porter (1972) and Wood (1980a) using $W_{Cr}=0.40 \cdot W_{Co}$. Considering the volcano as two truncated cones, we obtained a total volume of $1.17 \cdot 10^7$ m^3 for mean dimensions. We use 43.7% of the cone volumes as magma volume, an average percentage that was estimated by Mertes (1983) for W-Eifel scoria cones. We further assumed 10% of the erupted magma to have been deposited beyond the volcanic edifice. This is a conservative estimate when taking the inferred high volatile content of Herchenberg magma and moderate fragmentation of tephra into account. Head and Wilson (1989) relate the height of Strombolian eruption columns directly to the magma gas content. The Herchenberg eruption column was thus probably high compared to those of basanite/tephrite scoria cones of the E-Eifel. The occurrence of two distal melilite-nephelinitic tuffs in the key Pleistocene section of the Kärlich clay pit (Bogaard et al. 1989) as well as Miesenheim II also indicates that depositional fans from eruptions of such magmas may be widespread. A total magma volume (DRE) of $8.2 \cdot 10^6$ m^3 was obtained in this way.

Magma volumes of many other E-Eifel basanitic to tephritic scoria cones are larger by factors of 2–3, $2.8 \cdot 10^7$ m^3 for Karmelenberg volcano (Pier 1978), $2.3 \cdot 10^7$ m^3 for Rothenberg volcano (Karakuzu 1982), and $1.7 \cdot 10^7$ m^3 for the Southern Eiterkopf volcano (Prange 1984). The volume of Herchenberg, however, exceeds that of most scoria cones of the W-Eifel volcanic field (dominantly of nephelitinic to leucitic composition), where 90% of the scoria cones have magma volumes $<8 \cdot 10^6$ m^3 (Mertes 1983).

Morphology of essential clasts

Essential lapilli were subdivided mainly by morphology and vesicularity/porosity. The mean bulk rock density was determined for 50 clasts of each type using hydrostatic balance methods (Fig. 16). The particles were covered with a rubber-latex skin to seal the pores.

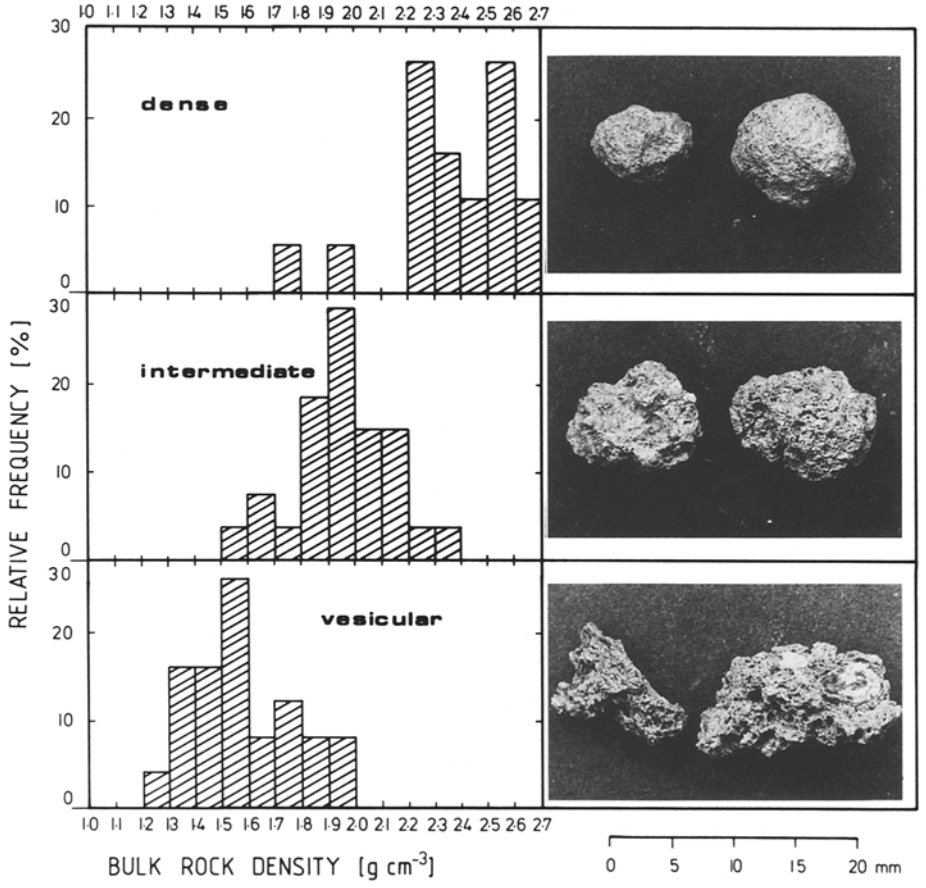

Fig. 16. Histograms showing relative frequency distributions of bulk densities of vesicular (A), intermediate density (B), and dense (C) lapilli in the -2Φ fraction of Herchenberg tephra. Photographs of representative specimens are shown in the right column

A) Vesicular lapilli. Mean bulk rock density, 1.5 g/cm^3; calculated mean porosity (for an assumed solid rock density of 2.9 g/cm^3), 46 vol% (range of 32–58 vol%). Many vesicles (up to several millimeters in diameter) are visible at the surface of the clasts, giving them a rough appearance. The lapilli are very angular to angular (Fig. 16), some are elongated.

B) Intermediate density lapilli. Mean bulk rock density, 1.95 g/cm^3; mean porosity, 32.8 vol.% (range of 20–46 vol%). The size and abundance of vesicles at the surface is much smaller than for clasts of type A. Few larger vesicles are restricted to the core of the clasts. The surface is less rough. Roundness is subangular to subrounded (Fig. 16).

C) Dense lapilli. Mean bulk rock density, 2.35 g/cm^3; mean porosity, 18.6 vol% (range of 9–32 vol%). Vesicles >0.5 mm are generally absent at the surface, roundness is subrounded to rounded (Fig. 16).

Ellipsoidal lapilli

Ellipsoidal lapilli are of type C and appear throughout the Herchenberg deposits, but are dominant components in the upper part of cone 1 and in cones 2 and 3. We obtained geometric parameters and bulk rock density from 50 ellipsoidal lapilli each of cone 1 and 2 de-

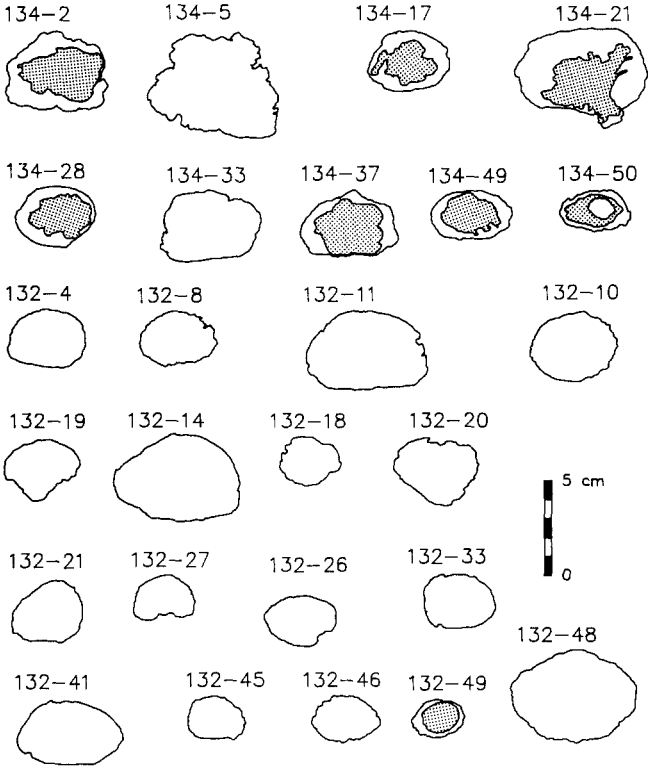

Fig. 17. Cross sections of representative, mostly smoothly contoured ellipsoidal lapilli (dense lapilli of type C). Shaded areas indicate vesicular portions, which are mostly restricted to the interiors. Samples 135-** taken from upper cone 1 (UC1), and samples 132-** from cone 2 (C2)

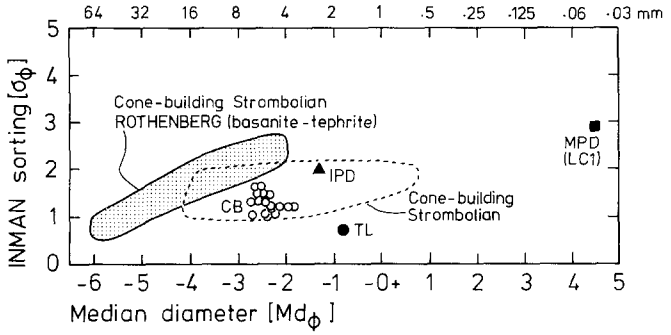

Fig. 18. Diagram of median diameter (Md_Φ) vs Inman sorting ($\sigma\Phi$) of Herchenberg tephra deposits. *IPD*, initial phreatomagmatic deposits; *MPD*, massive phreatomagmatic deposits of lower cone 1 (LC1); *CB*, cone-building stages; *TL*, top layers. Shaded field for basanite-tephrite Rothenberg cone-building Strombolian deposits after Houghton and Schmincke (1989). Field for cone-building Strombolian phases designated by broken line after Walker and Croasdale (1972)

posits. Aspect ratios range from 0.5 to 0.9, averaging around 0.68 in cone 1 and 0.74 in cone 2. Common to all ellipsoidal lapilli is a low porosity reflected in high bulk rock densities with an average of 2.18 g/cm^3 (ca. 24 vol% vesicles) in cone 1 and 2.56 g/cm^3 (ca. 11 vol% vesicles) in cone 2. Vesicular portions are normally restricted to the central portions of the lapilli (Fig. 17, e.g., 134-2, 134-17) in the case of cone 1. Their internal structure shows abundant evidence of fluid motion within the lapilli during eruption (Bednarz and Schmincke, in prep).

Grain size distribution

Herchenberg tephra differs from other, mostly basanitic to tephritic E-Eifel scoria cones due to its restricted grain size (lapilli range) and good sorting (Fig. 18). Twenty-five samples collected at locations 20–100 m outside the crater walls have Md_Φ values between -1.9 and -2.7 Φ (mean, -2.35 Φ; std dev., 0.23). Inman sorting σ_Φ ranges from 1.0 to 1.6 (mean 1.25; std dev., 0.18). We tried to take into account the common reversely graded bedding by channel sampling. Poorly sorted tuffs of phreatomagmatic origin in the initial deposits have Md_F values as high as 4.5 Φ and σ_Φ values up to 2.9. This very fine grain size is thought to be mainly due to the high content of non-juvenile Tertiary clay and silt material (estimated to be $>80\%$) deriving from the underlying strata of the volcano, rather than due to efficient fragmentation of juvenile material by thermal shock.

Another "extreme" grain size distribution is found in a sample of the late tephra with a Md_Φ of -0.8 Φ and a good sorting coefficient σ_Φ of 0.7.

Eruptive mechanisms

The Herchenberg eruptive history is summarized as follows (Fig. 6):

I) Initial stage. Mainly phreatomagmatic, poorly sorted massive tuffs and tuff breccias (channel facies); lapilli-size components are dominantly vesicular; formation of a maar-like crater; major crater wall collapse at the end of the initial stage leads to tectonic repetition of strata. Strombolian eruptions dominate the eastern parts of the volcano.

II) Rhythmic depositional cycle stage of lower cone 1 (mainly northwestern sector) grading into massive phreatomagmatic facies (northeastern and southern sectors). A depositional cycle of 2–3 characteristic bed types represents the rim facies of lower cone 1.

III) Main cone-building stage (upper cone 1, cone 2, cone 3). Mostly reversely graded layers, rich in dense ellipsoidal juvenile clasts. Increase of basal cone diameters by slumping; intrusion of 3 major dikes.

IV) Final stage (top layers). Phreatomagmatic eruptions generating accretionary lapilli layers, poorly sorted tuffs; scoriaceous lapilli at the end.

I) Initial phreatomagmatic eruptions of scoria cone volcanoes are common in the E and W Eifel volcanic fields (summaries in Schmincke 1977a, 1991; Mertes 1983), but have not commonly been described from other monogenetic volcano fields. We feel that the deep level of extensive quarrying in many of the E and W Eifel volcanoes simply give us a better insight into the entire evolution of a scoria cone. We suspect that initial phreatomagmatic phases are common because most basaltic dikes will cross a water table. The degree and style of interaction, however, will strongly depend on the local pre-eruptive geology, hydrology, and topography as well as on physical parameters (e.g., viscosity), gas content, and ascent velocity of the magma. The abundance of near surface Tertiary sediments, loess, soils, and tephra layers in the E-Eifel, which act as aquifers, may be equally important for the frequent occurrence of initial phreatomagmatic eruptions.

The abundant xenoliths ($>80\%$ by volume in single layers) of the initial deposits were derived almost entirely from the unconsolidated Tertiary clays, silts, sands, and gravels. Initial interaction of water and magma thus did not take place until the magma had reached the Tertiary-Devonian boundary about 20–25 m below the surface, an interpretation supported by the vesicular nature of the lapilli in the phreatomagmatic deposits and in intercalated strombolian lapilli layers. Near surface interaction between a mixture of vesicular lava blebs and expanding magmatic gas with water from the sediments led to violent phreatomagmatic eruptions because of the great volume difference between water and steam at low lithostatic pressures.

Early homogeneous Strombolian fallout deposits occur mainly in the southern and southeastern parts of the volcano. This indicates that beginning with the early stages of the eruptive activity, high level magma/water interaction was restricted to the northwestern parts of the volcano.

II) The most characteristic feature of the lower part of the northwestern sector of cone 1 is the cyclic deposition of tephra bed types a and b. Rare, though significant accretion structures against obstacles (Fig. 8) indicate that material (mostly bed types a) during this stage was repeatedly transported laterally from the crater by surges. The small size of some obstacles (< 10 cm; Fig. 8) is clear evidence for low energy (and probably high dilution) of these surges, at least in the unchannelled rim facies. This contrasts with frequent erosion of the crater wall crest (Fig. 7). This may result from (a) base surges which were erosive at their heads and depositional in their body and tail or (b) from lateral blasts preceeding the actual base surge. Alternatively, the outer slopes of LC1 may have been situated in the flow shadow region with the lower energy of the base surges as on the crater wall crest.

A radial facies change of type-a beds can be observed in a morphologic depression in the northeast and south (Fig. 4) toward a massive facies. This indicates that the surges were channelled and that the preferred direction of transport was northeastward and southward. Large xenolith blocks (up to 1 m) are concentrated in the massive facies and indicate high kinetic energy. The intercalated lapilli beds do not form distinct layers in the massive, proximal facies but separate irregular lenses indicating erosion and synsedimentary creep of this water-rich deposit. The outcrops of initial deposits at the southern side of the volcano I belong to a similar massive facies. A general topographic low in the southern part of Herchenberg (Figs. 2, 4) suggests a preferred southward transport of surges.

The eruptive cycle (simplified as surge - dense lapilli - scoriaceous lapilli) can be explained by iterative slumping of the unstable Cenozoic sediments into the crater area thus choking the conduit and simultaneously enabling repeated introduction of water directly into the magma-filled fissure. The eruptive sequence started with a shock wave eroding the crater wall. It was directly followed by a xenolith-rich base surge which transported the bulk of the material through preexisting channels (topographic lows or notches in the crater wall). We relate this sequence to varying lava levels in the conduit, permitting reflux of water toward the conduit in the Tertiary basement at low lava levels leading to phreatomagmatic eruptions when the lava level subsequently rose above the groundwater table leading to intimate water-magma contact and superheating of the water in a closed system. Devonian xenolith contents of up to about 10 wt% indicate that water-magma interaction (at least occasionally) also took place below the Tertiary-Devonian boundary. The beginning of a continuous Strombolian eruption generating fallout of more vesicular lapilli deposited on the top of each cycle is often marked by a population of relatively dense lapilli. Some lapilli deposited inside the crater wall were still hot enough to weld.

Partial crater collapse at the end of the initial stages and effective choking of the conduit led to the deposition of two prominent layers especially rich in large xenoliths, each followed by a characteristic layer of highly scoriaceous lapilli indicating re-opening of the vent and continuous Strombolian activity.

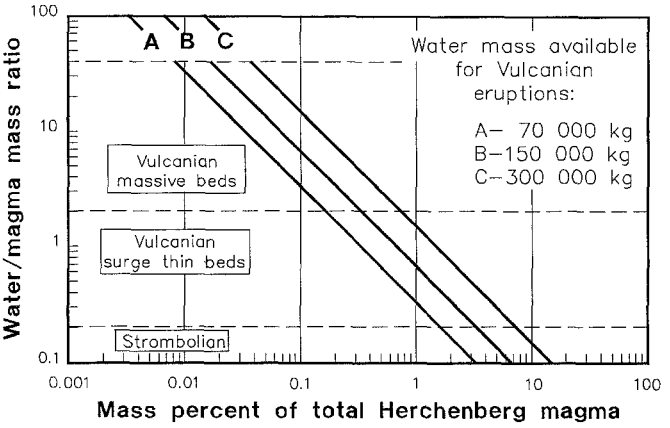

Fig. 19. Diagram showing relative proportion of total Herchenberg magma (assumed to be $2.4 \cdot 10^{10}$ kg) which could have had erupted at different water/magma mass ratios assuming that the total available water mass was (a) 70000 kg, (b) 150000 kg, or (c) 300000 kg. Boundaries for Strombolian, Vulcanian (surge thin bed), and Vulcanian (massive beds) after Wohletz (1983)

The primary external water source for phreatomagmatic eruptions during the early stages of the Herchenberg evolution was a 20-m-thick deposit of underlying Tertiary clays and sands (Ahrens 1929). Assuming 200–400 l of water per m^3 in the Tertiary sediments (natural water contents of unconsolidated sediments after Terzaghi and Peck 1967) there was up to $0.7 \cdot 10^5$ m^3 to $1.4 \cdot 10^5$ m^3 water available in the crater area of cone 1. Experiments by Wohletz (1980, 1983) showed that deposition of massive tuff beds by phreatomagmatic eruptions requires minimum water/magma mass ratios of approximately 2. Assuming even twice this maximum water volume, less than 1 wt% of the total Herchenberg magma mass could have erupted to produce massive tuff beds (Fig. 19). This is in accordance with their low overall abundance.

III) The main Strombolian cone-building stages of Herchenberg volcano (upper cone 1, cone 2, cone 3) are characterized by a significant decrease in vesicular lapilli content during their evolution. Simultaneously the relative abundance of dense spheroidal lapilli, which themselves become denser from cone 1 to cone 2, continuously increases. The general paucity of xenoliths (< 1%) is also striking even in the early deposits of the later cones 2 and 3. Individual marker beds (10–30-cm-thick tuff, tuffaceous lapilli, and accretionary lapilli layers) contain almost exclusively Devonian xenoliths (up to 30 wt%).

At the end of LC1 formation, the conduit system in the Tertiary sediments extending into the Devonian basement was well-established and stable while the lava level and the level of lava disruption had sunk. Occasional phreatomagmatic pulses during formation of UC1 are indicated by Tertiary xenolith-rich layers in the southern sector. During this period, the northern crater wall of cone 1 was about 20–30 m higher than the

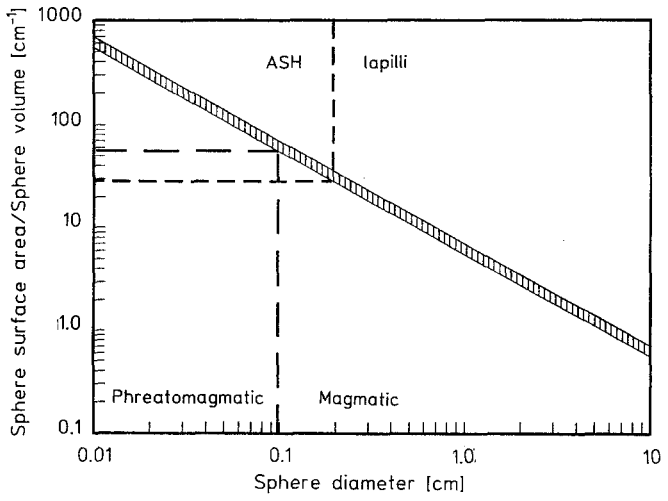

Fig. 20. Diagram showing effective surface area of tephra particles depending on their mean diameter. *Short broken lines* indicate the boundary between lapilli- and ash-size particles (2 mm). *Long broken lines* indicate the minimum effective surface area required for heat transfer effective enough to allow fast expansion of external water and thus phreatomagmatic eruptions according to Wohletz (1983)

southern crater wall. The lack of Tertiary clasts in the northern sector of UC1 may thus indicate their ejection on very low angle trajectories, which did not clear the northern crater wall.

Temporarily higher local temperatures and accumulation rates during eruption of cone 2 deposits, which led to the formation of a small rootless spatter flow, may be related to lower gas contents in the lower parts of the Herchenberg magma column (cf. Head and Wilson 1989). This is paralleled by the increasing abundance of high density ellipsoidal lapilli in cones 2 and 3 (Figs. 9, 14).

This contrasts with a relatively low depositional temperature of near-vent tephra during most of the eruptive history of Herchenberg volcano. We believe that the reason for this probably lies in small grain sizes even in these near-vent deposits which cool much more rapidly than large spatter because the effective surface area of particles increases exponentially with decreasing particle diameter (Fig. 20). We assume that Strombolian eruption columns during the activity of Herchenberg volcano were high compared to those of basanite-tephrite cones due to high inferred volatile contents (especially CO_2) of Herchenberg magmas while mass eruption rates of magma were low. Substantial cooling of the erupting particles by external water (steam) may have been an additional important factor in the core area of cone 1 where eruptions were repeatedly modified by external water.

Occasional choking of the vent below the Tertiary-Devonian boundary facilitated admixing of deeper level water and thus led to the deposition of phreatomagmatic marker beds characterized by abundant Devonian xenoliths and dense angular juvenile clasts. The high water content of these breccia tuffs is indicated by plastic deformation upon bomb impact. Also characteristic is the subsequent deposition of "unusual" scoriaceous lapilli layers rich in vesicular type-A lapilli.

The paucity of country rock clasts in the early deposits of cones 2 and 3 is striking, though the "cores" of both are deeply exposed, which is most likely due to either of two causes:

1) The eruptive center of the initial eruptions of the Herchenberg volcano was a NW-SE-trending fissure. The conduit for cones 2 and 3 was cleared in the very early stages of the eruption. This model is partly supported by the occurrence of strong crater collapse tectonics in the initial deposits (Ia) about 300 m away from the actual eruptive center of cone 1. After development of an initial fissure about 500 m long, eruptive activity would have extended to the northwest and later migrated to the southeast, where the crater area had already been cleared of the Tertiary basement.

2) The spatial distribution of preserved Tertiary sediments is related to a local graben-like tectonic structure whose boundaries are unknown. If one of these boundaries would have intersected the fissure, the southeastern center may well have been located outside this small basin. This would most easily explain the lack of phreatomagmatic deposits and Tertiary xenoliths in cones 2 and 3.

IV) Late-stage phreatomagmatic eruptions from a low lava level in the Devonian basement may have been facilitated when longer pauses between eruptive intervals and deeper lava levels enabled groundwater to recharge and migrate to the conduit.

Terminal scoriaceous lapilli layers, some forming widespread regional marker beds, are common in E-Eifel scoria cones (Schmincke 1991). We believe that the top layers originated from within the Herchenberg volcanic structure because (a) there is no indication for a long depositional hiatus and (b) the layers are chemically and mineralogically identical to the rest of the Herchenberg. The exact location of the eruptive center (cone 1 or 2-3) is unknown. The maximum thickness of top layers is, however, exposed on the flanks of cone 1. It is thus likely that they originated from the northwestern part of Herchenberg volcano.

Conclusions

Scoria cones are produced by a large variety of Hawaiian or Strombolian eruptions (e.g., Macdonald 1972; Thorarinsson et al. 1973; Self et al. 1974; Blackburn et al. 1976; Williams and McBirney 1979; Fedotov et al. 1980; Fisher and Schmincke 1984). The style of basaltic eruption is controlled by internal parameters such as chemical composition, volatile contents, and eruptive rates of magma and external factors such as local and regional stress regimes, the density structure of the crust, and the scale and influence of external water (e.g., Chouet et al. 1974; Lorenz 1975; Schmincke 1977a; Nakamura 1981; Wilson and Head 1981; Kokelaar 1983; Wohletz 1983; Vergniolle and Jaupart 1986; Head and Wilson 1989). Substantial variations in the grain size characteristics, morphology, and vesicularity

of juvenile clasts and abundance of country rock fragments in tephra deposits of E-Eifel scoria cones have been mainly attributed to the varying degrees and different modes of interaction between magma and meteoric water (Schmincke 1977a; Houghton and Schmincke 1986, 1989). Extremely high eruption rates and lava flow volumes of the Ettringer Bellberg volcano in the Eifel have been related to a long eruptive fissure following a regional fault of Cenozoic age (Sobczak 1987; Schmincke 1991).

We find the variable chemical compositions, volatile contents, and related physical properties of mafic to intermediate E-Eifel magmas to be equally important parameters controlling eruptive styles, structures of scoria cones, and characteristics of tephra deposits. We thus distinguish two end member:

a) Scoria cones, like Herchenberg and the nearby Leilenkopf (Bednarz 1982), constructed from highly silica-undersaturated magmas (nephelinites and leucitites) which have not been drastically fractionated in mid- or upper-crustal magma chambers (Table 1). This type of volcano is characterized by relatively high degrees of magma fragmentation resulting in the dominance of lapilli layers over breccia deposits even in the near-vent facies. Intense welding of the cores of eruptive centers is restricted to a relative small area about 50–100 m in diameter in the Herchenberg area and 80–100 m in the Leilenkopf area. We interprete these two phenomena to result from a high ratio of gas volume flux to magma flux during eruption of Herchenberg and Leilenkopf volcanoes, which is for instance dependant on the primary volatile concentration of the magma and the abundance of different volatile species. For Herchenberg magmas, we infer high proportions of CO_2 (<4 wt%; Bednarz and Schmincke, in prep) whose solubility even in alkalic, silica-undersaturated magmas is very low and strongly pressure dependant. High CO_2 concentrations, which are confirmed by the occurrence of carbonatite segregations at Herchenberg (Bednarz and Schmincke, in prep), will lead to early, deep bubble formation while the low viscosity of the magma facilitates bubble coalescence. This may create large bubbles which rise faster through the crust than their "host" magmas resulting in a very inhomogeneous bubble size distribution ("bubbly slug flow") and a high ratio of gas volume to magma volume in the eruption (Vergniolle and Jaupart 1986).

The low viscosity of alkali-rich, silica-undersaturated magmas (average of 70 poise at 1100° C for E- and W-Eifel after Bednarz and Schmincke, in prep) further decreases the diameter of stable liquid "drops" during the eruption when these are subject to external forces, e.g. acceleration. Higher viscosities may delay the resulting deformation until the relative air velocity drops below a critical value or until ongoing cooling and polymerization of the melt stabilize the lava drops (lapilli; Bednarz and Schmincke, in prep).

b) Most good exposures of mafic volcanoes in the E-Eifel are found in basanitic to tephritic scoria cones. Lower degrees of magma fragmentation than in type-a scoria cones is evident from the abundance of breccia deposits and scarcity of lapilli layers (Fig. 18). Lower eruptive columns and lower gas volume/magma volume ratios due to lower primary volatile concentrations and lower relative rise velocities of magma and bubbles result in wide agglutinated crater areas in which strong welding has diameters of up to 250 m (e.g., Rothenberg, Sattelberg, Karmelenberg). Higher magma viscosities (average of 230 poise at 1100° C for E-Eifel basanites after Bednarz and Schmincke, in prep) delay post-eruptive deformation of liquid particles thus increasing their stable diameters.

Table 1. Selected XRF analyses of Herchenberg melilite-nephelinitic lavas. Analyses of Rothenberg tephrite (S387) and basanite (R09; from Karakuzu 1982) are included for comparison. Oxides as weight percent, trace elements as ppm

	Herchenberg		Rothenberg	
Sample	125	120	S387	R09
SiO_2	38.50	39.80	44.30	43.70
TiO_2	2.87	3.19	2.76	2.83
Al_2O_3	13.00	13.80	15.80	13.00
Fe_2O_3	8.43	10.30	5.05	6.68
FeO	1.99	1.36	6.01	3.83
MnO	0.20	0.21	0.24	0.18
MgO	7.89	8.99	5.31	9.12
CaO	13.50	14.20	10.70	11.70
Na_2O	2.73	3.62	3.80	2.97
K_2O	1.77	3.57	3.84	3.32
P_2O_5	0.73	0.69	0.86	0.56
H_2O	4.53	0.36	0.59	0.30
CO_2	2.91	0.04	0.11	0.12
Total	99.17	99.87	99.80	98.61
S	0.09	0.02	0.07	0.02
Cl	0.03	0.02	0.04	0.01
Cr	131	158	44	236
Co	52	56	46	64
Ni	74	94	32	122
Cu	61	87	57	77
Zn	77	85	97	82
Rb	165	79	90	86
Sr	959	1244	1229	878
Y	12	32	31	22
Zr	259	259	359	275
Nb	127	132	115	78
Ba	1015	1347	999	1084

Acknowledgements. Field and analytical work were financially supported by the BMFT project 03E-4236-A and grants from the Deutsche Forschungsgemeinschaft Schm 250/38-1. We thank H Niephaus who run the X-ray spectrometer and A Fischer for her photographic work. We gratefully acknowledge the detailed reviews of JG Moore and BF Houghton which helped to improve the manuscript.

References

Ahrens W (1929) Das Tertiär im nördlichen Laacher-See-Gebiet. Jahrb Preuß Geol Landesanst 50:332–370

Ahrens W (1930) Geologische Skizze des Vulkangebietes des Laacher Sees. Jahrb Preuß Geol Landesanst 51:130–140

Bednarz U (1982) Geologie und Petrologie der spätquartären Vulkane Herchenberg, Leilenkopf und Dümpelmaar (nördliches Laacher-See-Gebiet). Diplom-thesis (Diplomarbeit) Ruhr-Universität Bochum (unpubl):1–298

Bednarz U, Schmincke HU (1990a) The formation of dense ellipsoidal lapilli in scoria cones of the East- and West-Eifel volcanic fields (FRG) (in prep)

Bednarz U, Schmincke HU (1990b) Petrology and geochemistry of the Quaternary melilite-nephelinite-carbonatite Herchenberg scoria cone (E-Eifel, W-Germany) (in prep)

Blackburn EA, Wilson L, Sparks RSJ (1976) Mechanisms and dynamics of strombolian activity. J Geol Soc 132:429–440

Bogaard Cvd, Bogaard Pvd, Schmincke HU (1989) Quartärgeologisch-tephrostratigraphische Neuaufnahme und Interpretation des Pleistozänprofils Kärlich. Eiszeitalter und Gegenwart 39:62–86

Bogaard Pvd, Schmincke HU (1985) Laacher See Tephra-A widespread isochronous Late Quaternary tephra layer in Central and Northern Europe. Geol Soc Am Bull 96:1554–1571

Bogaard Pvd, Hall CM, Schmincke HU, York D (1987) $^{40}Ar/^{39}Ar$ laser dating of single grains: Ages of Quaternary tephra from the East Eifel volcanic field, FRG. Geophys Res Lett 14:1211–1214

Chouet BN, Hamisevicz N, McGetchin TR (1974) Photoballistics of volcanic jet activity at Stromboli, Italy. J Geophys Res 79:4961–4975

Duda A, Schmincke HU (1978) Quaternary basanites, melilite nephelinites and tephrites from the Laacher See Area (Germany). N Jb Miner Abh 132:1–33

Duffield WA, Bacon CR, Roquemore GR ((1979) Origin of reverse-graded bedding in air-fall pumice, Coso Range, California. J Volcanol Geotherm Res 5:35–48

Fedotov SA, Chirkov AM, Gusev NA, Kovalev GN, Slezin YB (1980) The large fissure eruption in the region of Plosky Tolbachik Volcano in Kamchatka, 1975–1976. Bull Volcanol 43:47–60

Fisher RV, Schmincke HU (1984) Pyroclastic rocks. Springer Berlin Heidelberg New York Tokyo, pp 1–472

Head III JW, Wilson L (1989) Basaltic pyroclastic eruptions: influence of gas-release patterns and volume fluxes on fountain structure, and the formation of cinder cones, spatter cones, rootless flows, lava ponds and lava flows. J Volcanol Geotherm Res 37:261–271

Houghton BF, Schmincke HU (1986) Mixed deposits of simultaneous Strombolian and phreatomagmatic volcanism (Rothenberg volcano, East Eifel). J Volcanol Geotherm Res 30:117–130

Houghton BF, Schmincke HU (1989) Rothenberg scoria cone, East Eifel: a complex Strombolian and phreatomagmatic volcano. Bull Volcanol 52:28–48

Karakuzu F (1982) Teil I: Aufbau und Entstehung der spätquartären Vulkane Dachsbusch und Rothenberg in der Osteifel. Teil II: Geologische und petrologische Entwicklung der Vulkane Rothenberg, Dachsbusch und Wehrer Kessel. Diplomthesis (Diplomarbeit) Ruhr-Universität Bochum (unpubl):1–215

Kokelaar BP (1983) The mechanism of Surtseyan volcanism. J Geol Soc London 140:939–944

Lorenz V (1975) Formation of phreatomagmatic maar diatreme volcanoes and its relevance to kimberlite diatremes. Phys Chem Earth 9:17–27

Macdonald GA (1972) Volcanoes. Prentice-Hall Inc, Englewood Cliffs, New Jersey, pp 1–510

McGetchin TR, Settle M, Chouet BA (1974) Cinder cone growth modeled after Northeast Crater, Mount Etna, Sicily. J Geophys Res 79:3257–3272

Mertes H (1983) Aufbau und Genese des Westeifeler Vulkanfeldes. Bochumer geol geotechn Arb 9:1–415

Meyer W, Stets J (1975) Das Rheinprofil zwischen Bonn und Bingen. Z dt Geol Ges 126:15–29

Nakamura K (1981) Two basic types of volcanoes – polygenetic and independant monogenetic group of volcanoes, and tectonic stress field (abstract). In: Abstracts of the 1981 IAVCEI Symposium – arc volcanism – The Volcanological Society of Japan and the International Association of Volcanology and Chemistry of the Earth's Interior:251

Pier R (1978) Teil 1: Aufbau und Entstehung des spätquartären Basanitvulkankomplexes Karmelenberg. Teil 2: Sedimentologie und Petrographie der Pyroklastika und Laven des Karmelenberges (E-Eifel). Diplom-thesis (Diplomarbeit) Ruhr-Universität Bochum (unpubl), pp 1–139

Porter SC (1972) Distribution, morphology and size frequency of cinder cones on Mauna Kea volcano, Hawaii. Geol Soc Am Bull 83:3607–3612

Prange C (1984) Die vulkanologische, tektonische und geochemische Entwicklung der quartären Eiterkopfvulkane, SE-Eifel. Diplom-thesis (Diplomarbeit) Ruhr-Universität Bochum (unpubl):1–236

Schmincke HU (1977a) Phreatomagmatische Phasen in quartären Vulkanen der Osteifel. Geol Jb A39:1–48

Schmincke HU (1977b) Eifel-Vulkanismus östlich des Gebietes Rieden-Mayen. Fortschr Mineral 55:1–31

Schmincke HU (1982) Vulkane und ihre Wurzeln. Rhein Westf Akad Wiss Westd Verlag Opladen N315, pp 35–78

Schmincke HU (1991) Die quartären Vulkanfelder der Eifel. Schweizerbart'sche Verlagsbuchhandlung Stuttgart (in press)

Schumacher R (1988) Aschenaggregate in vulkaniklastischen Transportsystemen. PhD-thesis (Ruhr-Universität Bochum), pp 1–140

Schumacher R, Schmincke HU (1990) The lateral facies of ignimbrites at Laacher See volcano. Bull Volcanol 52:271–287

Self S, Sparks RSJ, Booth B, Walker GPL (1974) The 1973 Heimaey strombolian scoria deposit, Iceland, Geol Mag 111:539–548

Sobczak G (1987) Vulkanologische und geochemische Entwicklung der spätquartären Bellerberg Vulkangruppe (Osteifel). Diplom-thesis (Diplomarbeit) Ruhr-Universität Bochum (unpubl), pp 1–215

Terzaghi K, Peck RB (1967) Soil Mechanics in Engineering Practice. Wiley London, pp 1–729

Thorarinsson S, Steinthorsson S, Einarsson T, Kristmannsdottir H, Oskarsson N (1973) The eruption on Heimaey, Iceland. Nature 241:372–375

Vergniolle S, Jaupart C (1986) Separated two-phase flow and basaltic eruptions. J Geophys Res 91:12842–12860

Viereck L (1984) Geologische und petrologische Entwicklung des pleistozänen Leuzitit-Leuzitphonolith-Vulkankomplexes Rieden, Osteifel. Bochumer Geol Geotechn Arb 17:1–337

Walker GPL, Croasdale R (1972) Characteristics of some basaltic pyroclastics. Bull Volcanol 35:303–317

Williams H, McBirney AR (1979) Volcanology. Freeman, Copper & Cp, San Francisco, pp 1–397

Wilson L, Head III JW (1981) Ascent and eruption of basaltic magma on the earth and moon. J Geophys Res 86:2971–3001

Wörner G, Schmincke HU (1984) Mineralogy and geochemical evolution of the Laacher See magma chamber. J Petrol 25:805–835

Wohletz KH (1980) Explosive hydromagmatic volcanism. PhD-thesis Arizona State University (unpubl), pp 1–231

Wohletz KH (1983) Mechanisms of hydrovolcanic pyroclast formation: grain-size, scanning electron microscopy, and experimental studies. J Volcanol Geotherm Res 17:31–63

Wood CA (1980a) Morphometric evolution of cinder cones. J Volcanol Geotherm Res 7:387–413

Wood CA (1980b) Morphometric analysis of cinder cone degradation. J Volcanol Geotherm Res 8:137–160